Input output linearization on the underactuated H-drive

Input output linearization on the underactuated H-drive

H.A. Pastink

DCT.2003.85

Report internship

Coach: Prof.dr. H. Nijmeijer

Eindhoven University of Technology
Department of Mechanical Engineering
Dynamics and Control group

Eindhoven, September 23, 2003

Summary

The H-drive is a servo system consisting of perpendicular axes in the horizontal plane on which linear motors can translate. In order to make the H-drive underactuated, a link is mounted on top of one of its linear motors. The link is not actuated, it is free to rotate.

In order to cancel the disturbing effects of the rotating link on the performance of the H-drive as a servo system, input output linearization (further referred to as IO linearization) is implemented. The IO linearizing control law is based on a rigid body model for the H-drive. The model does not include horizontal tilt motion of the translating axis. Merely friction in the bearing of the link has been accounted for.

Choosing the actuated DOFs as outputs, the relative degree is well defined. For this choice of output functions, the zero and tracking dynamics simply coincide with the link's motion that arises when the control goals for the actuated DOFs have been realized. The stability of the tracking dynamics depends on the reference trajectories imposed. In case of the zerodynamics, the angular velocity of the link will asymptotically decay to zero. The link will come at rest at some arbitrary position.

An additional servo system is employed to control the H-drive. By doing so, the so called "virtual internal model following control" approach is implemented. The additional servo system prevents tilt motion of the translating axis. Moreover, the additional servo controller is able to suppress unmodelled phenomena such as friction and cogging forces.

Stabilization and tracking experiments are performed. Simulation results agree quite well with the experimental results in case of the actuated DOFs. Because the effects of static friction are underestimated using a continuous friction model, the link's motion is not well predicted by the simulations. The currents measured are significantly larger than the currents simulated. Reason for this are disturbances such as friction and cogging.

Experiments show that IO linearization is successfully implemented. The underactuated H-drive proves to be a system very suitable for the application of IO linearization. The actuated DOFs are globally stabilized using linear pole placement techniques. Thanks to the additional servo controller, a robust form of IO linearization is obtained. Due to a servo error in the low level servo loop, no exact IO linearization can be obtained.

The main recommendation is to remove the need for the additional servo controller by implementing a more accurate model for the H-drive. This model should for example account for horizontal tilt motion and should include a suitable model for friction present on the X and Y axes.

Contents

Chapter 1

Introduction

Underactuated mechanical systems are defined as systems having less inputs than degrees of freedom. These systems frequently appear in daily life, examples of them are surface vessels, helicopters and underactuated manipulators. Within the scope of research in the control of underactuated mechanical systems in the *Dynamics and Control* group, the H-drive servo system is adjusted. On top of one of its linear motors, a link is mounted. The link is not actuated; it is free to rotate.

This internship comprises three subjects related to the underactuated H-drive. First, a range of experiments using the controller designed in [1] is performed. The main goal of these experiments was to diminish the disturbance that arises when the link's plane of rotation is not exactly horizontal. Second, the controllability properties of the linearization of a model including horizontal tilt motion are investigated. Both the first and second subject are carried out in close cooperation with W.T. Oud. The third and main subject is the implementation of IO linearization on the underactuated H-drive. In this report, emphasis is placed on the latter subject.

Controlling the underactuated H-drive involves severe difficulties. Referring to [2], the system is controllable. The linearization is not controllable because gravity exerts no influence on the link. Because no linear controller can stabilize the underactuated H-drive, the possibilities of nonlinear control methods for controlling the underactuated H-drive are being explored within the *Dynamics and Control* group.

The Ph.D. project of E. Aneke was dedicated to the control of the unactuated link itself. In [1] a controller in second order chained form is successfully applied to the underactuated H-drive. The aim of this internship is to develop a control strategy that cancels the disturbing effects of the rotating link on the other DOFs. This disturbance will become significant when a substantial mass is mounted on the link. A control strategy that is very well capable of cancelling nonlinearities, is input output linearization (further referred to as IO linearization). IO linearization is a method that makes the input output behavior of a nonlinear system linear by feedback. Next, linear pole placement techniques can be applied to globally stabilize the input output behaviour of the system.

Chapter 1 starts with an introduction to the theory on IO linearization. In chapter 2, the equations of motion for the H-drive on which the IO linearization will be based are discussed. Furthermore, an IO linearizing control law will be derived. Also the control structure in which IO linearization will be embedded is discussed. In order to investigate the properties of the control strategy developed, simulations and experiments are performed. Simulation and experimental results of a stabilization and a tracking experiment will be discussed in Chapter 3. Hereafter, conclusions and recommendations are made. The subjects that have been carried out in co-operation with W.T. Oud are included in the Appendices. The improvements made to the H-drive as an experimental setup are discussed in the first appendix. In the second appendix, the controllability properties of the linearization of a model including horizontal tilt motion are discussed.

Chapter 2

Theory on IO linearization

IO linearization is a control strategy that makes the input output behavior of a nonlinear system globally linear by using a specific state feedback control law. The method totally differs from the Jacobian linearization of a nonlinear system. Before applying the strategy on the H-drive with link, a general introduction to the subject of IO linearization will be given. Merely the MIMO case will be treated, the SISO case (which follows directly from the MIMO case) will be omitted here. Consider a square MIMO system, i.e. a system that has an equal number of inputs and outputs, given by:

$$\begin{aligned} \dot{x} &= f(x) + g_1(x)u_1 + \ldots + g_p h_p(x) \\ y_1 &= h_1(x) \\ &\vdots \\ y_p &= h_p(x) \end{aligned} \tag{2.1}$$

Differentiating the output y_j with respect to time, one obtains:

$$\begin{aligned} \dot{y}_j &= \frac{\partial h_j}{\partial t} = \frac{\partial h_j}{\partial x}\frac{\partial x}{\partial t} = \frac{\partial h_j}{\partial x} f(x) + \sum_{i=i}^{p} \frac{\partial h_j}{\partial x} g_i(x) u_i \\ &:= L_f h_j(x) + \sum_{i=1}^{p} L g_i h_j(x) u_i \end{aligned} \tag{2.2}$$

Here, $L_f h_j(x)$ and $L_{g_i} h_j(x)$ are called the Lie derivatives of h_j with respect to f and g_i respectively. If at least one input appears in the first derivative of y_j, thus if $[L_{g_1} h_j(x) \ldots L_{g_p} h_j(x)] \neq [0 \ldots 0] \quad \forall \quad x$, the output y_j is said to have relative degree 1. The case in which $[L_{g_1} h_j(x) \ldots L_{g_p} h_j(x)] \neq [0 \ldots 0]$ for some subset of x will not be considered here. In that case, the relative degree is not well defined. If $[L_{g_1} h_j(x) \ldots L_{g_p} h_j(x)] = [0 \ldots 0]$, i.e. no input appears in the first derivative, (2.2) is differentiated once more, one then obtains:

$$\ddot{y}_j = L_f^2 h_j(x) + \sum_{i=1}^{p} L g_i L_f h_j(x) u_i \tag{2.3}$$

If $[L_{g_1}L_f h_j(x) \dots L_{g_p}L_f h_j(x)] \neq [0 \dots 0] \quad \forall \quad x$, the output y_j has relative degree two. In general, if α_j is the smallest integer such that at least one of the inputs u_i appears in the α_j-th time derivative of y_j, this output is said to have relative degree α_j. By determining subsequent Lie derivatives for all output functions, a p x 1 matrix $N(x)$ given by

$$N(x) = \begin{bmatrix} L_f^{\alpha_1} h_1 \\ \vdots \\ L_f^{\alpha_p} h_p \end{bmatrix} \tag{2.4}$$

and a p x p matrix A defined as

$$A(x) = \begin{bmatrix} Lg_1 L_f^{\alpha_1 - 1} h_1 & \dots & Lg_p L_f^{\alpha_1 - 1} h_1 \\ \vdots & \ddots & \vdots \\ Lg_1 L_f^{\alpha_p - 1} h_p & \dots & Lg_p L_f^{\alpha_p - 1} h_p \end{bmatrix} \tag{2.5}$$

can be established. The system's *vector* relative degree r is given by $\alpha_1, \alpha_2 \dots \alpha_p$. The vector of output derivatives can now be denoted as:

$$\begin{bmatrix} y_1^{(\alpha_1)} \\ \vdots \\ y_p^{(\alpha_p)} \end{bmatrix} = N(x) + A(x) \begin{bmatrix} u_1 \\ \vdots \\ u_p \end{bmatrix} \tag{2.6}$$

Provided that the matrix $A(x)$ is regular, a state feedback control law given by

$$u = A^{-1}(x)N(x) + A^{-1}(x) \begin{bmatrix} \nu_1 \\ \vdots \\ \nu_p \end{bmatrix} \tag{2.7}$$

linearizes the input output behaviour. A system that is linear from input ν_j to output y_j results:

$$\begin{bmatrix} y_1^{(\alpha_1)} \\ \vdots \\ y_p^{(\alpha_p)} \end{bmatrix} = \begin{bmatrix} \nu_1 \\ \vdots \\ \nu_p \end{bmatrix} \tag{2.8}$$

Note that the situation in which the relative degree is not well defined for some output causes $A(x)$ to become singular. In that case, the input will become arbitrarily large. In addition to being linearized, the system (2.8) is *decoupled*. Therefore, each output y_j can be separately stabilized using an additional controller ν_j. The m-th time-derivative of the tracking error e_j is defined as

$$e_j^{(m)} = y_j^{(m)} - y_{j_{ref}}^{(m)} \tag{2.9}$$

A ontrol law that stabilizes y_j is given by

$$\nu_j = y_{j_{ref}}^{(\alpha_j)} - k_{1,j} e_j^{(\alpha_j - 1)} - k_{2,j} e_j^{(\alpha_j - 2)} \dots - k_{\alpha,j} e_j \tag{2.10}$$

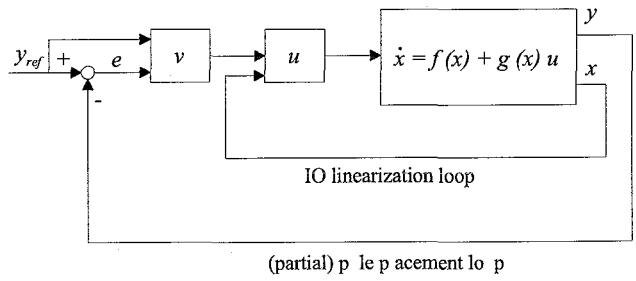

Figure 2.1: general structure of IO linearization. The system given by $f(x), g(x)$ is IO linearized by u, the error dynamics are partially (depending on the relative degree) stabilized by ν.

Finally, in figure 2.1, the structure of IO linearization is schematically depicted. After the IO linearizing control law has been derived, a coordinate transformation to the so called normal form is possible. The first $\alpha_1 + \alpha_2$ coordinates from this transformation are chosen the following way:

$$\begin{array}{rclcrcl} z_1(x) &=& h_1(x) & & z_{\alpha_1+1}(x) &=& h_2(x) \\ z_2(x) &=& L_f h_1(x) & & z_{\alpha_1+2}(x) &=& L_f h_2(x) \\ \vdots & & & , & \vdots & & \\ z_{\alpha_1}(x) &=& L_f^{\alpha_1-1} h_1(x) & & z_{\alpha_1+\alpha_2}(x) &=& L_f^{\alpha_2-1} h_2(x) \end{array} \tag{2.11}$$

Up to the r-th coordinate, $r = \alpha_1 + \alpha_2 + \ldots + \alpha_p$, coordinates can be defined this way. Depending on the relative degree, one must complete the coordinate transformation by $n - r$ coordinates. The choice for these coordinates is nontrivial; the transformation must be regular. The remaining coordinates are given by

$$z_{r+1}(x) = \eta_1(x), \quad \ldots \quad z_n(x) = \eta_{n-r}(x) \tag{2.12}$$

The dynamics represented within the z domain are:

$$\begin{array}{rclcrclcrcl} \dot{z}_1 &=& z_2 & & \dot{z}_{\alpha_1+1} &=& z_{\alpha_1+2} & & \dot{z}_{r+1}(x) &=& \dot{\eta}_1(x) \\ \dot{z}_2 &=& z_3 & & \dot{z}_{\alpha_1+2} &=& z_{\alpha_1+3} & & \dot{z}_{r+2}(x) &=& \dot{\eta}_2(x) \\ & \vdots & & , & & \vdots & & \ldots, & & \vdots & \\ \dot{z}_{\alpha_1}(x) &=& \nu_1 & & \dot{z}_{\alpha_1+\alpha_2}(x) &=& \nu_2 & & \dot{z}_n(x) &=& \dot{\eta}_{n-r}(x) \end{array} \tag{2.13}$$

The derivatives of $\eta_1(x) \ldots \eta_{n-r}(x)$ might be strongly nonlinear in $z_1, z_2, \ldots, z_n$ and in $\nu_1, \nu_2, \ldots, \nu_p$. After achieving a certain control task (i.e. the tracking error has vanished), dynamics on $\mathbf{R}^{n-r}$ remain. This part of the dynamics is unobservable from the outputs of the system. Depending on the type of control task, i.e. tracking or stabilization, these dynamics are called tracking dynamics, respectively zero dynamics. A system is said to be (locally) minimum phase when the origin of the tracking/zero dynamics is a (locally) stable equilibrium point. Obviously, a beneficial application of IO linearization requires the tracking and/or zero dynamics to be minimum phase. More detailed information on the subject of IO linearization can be found in [4].

Chapter 3

IO linearization on the H-drive

First, the equations of motion used to model the H-drive with will be discussed. Hereafter, the theory on IO linearization as presented in the foregoing chapter will be applied. Finally, the control structure in which IO linearization will be embedded is discussed.

3.1 Equations of motion

Figure 3.1 shows the setup of the H-drive. The H-drive is a servo system that consists

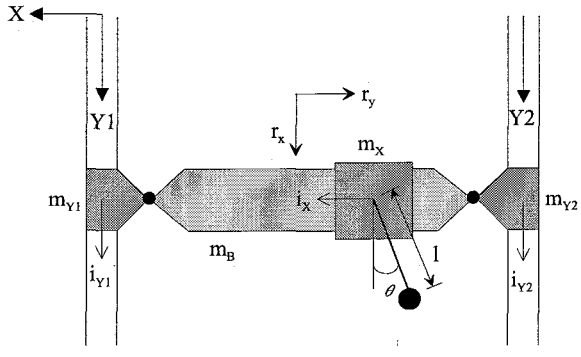

Figure 3.1: Schematic representation of the H-drive setup. The machine coordinates are denoted by X, Y_1 and Y_2, the link coordinates are given by r_x, r_y and θ. Note that Y_1 and Y_2 are not necessarily equal as is the case here.

of three axes on which linear motors can translate. The parallel axes Y_1 and Y_2 guide the motors m_{Y_1} and m_{Y_2} whose positions are controlled by the currents i_{Y_1} and i_{Y_2} respectively. The motors translating in Y direction are interconnected by a beam, the X axis. The X-axis guides the motor m_X which is controlled by the current i_X. The X-axis is mounted to the Y motors by means of elastic joints that allow small rotations in the horizontal plane. Due to possible tilt of the X beam, the positions Y_1 and Y_2 are

not necessarily equal. However, because of the servo task of the H-drive, the positions Y_1 and Y_2 will be controlled to follow the same reference trajectory. As a consequence, the positions Y_1 and Y_2 are assumed to be equal. The average of Y_1 and Y_2 will be denoted by Y, the average of i_{Y_1} and i_{Y_2} is consequently given by i_Y.

Two sets of coordinates are used to describe the H-drive's motion. One set is called the machine coordinates and consists of X, Y and θ plus their time-derivatives. This coordinate system will be used to indicate the positions of the X and Y motors. The other set of coordinates, the link coordinates, is denoted by r_x, r_y and θ and their accompanying time-derivatives. The latter set is obtained by a simple linear transformation of the machine coordinates:

$$r_x = -X - 0.3 \quad , \quad r_y = Y - 0.5 \tag{3.1}$$

By means of the coordinate transformation, the origin of the link coordinates can be defined at the center of the H-drive setup. The H-drive with the additional rotational link is an underactuated mechanical system: the number of DOFs (r_x, r_y, θ) exceeds the number of inputs (i_X, i_Y).

The H-drive's equations of motion have been derived using the method of Lagrange. For the derivation, a few assumptions have been made. First of all, the H-drive is assumed to consist of rigid bodies. Second, the position of masses m_{Y_1} and m_{Y_2} are assumed to be equal. Furthermore, the friction present on the X-axis and the Y-axes are assumed to be compensated for by the servo controllers of the linear motors. Disturbances such as cogging have not been taken into account. Finally, the H-drive is modelled by the following equations of motion:

$$\begin{array}{rcrcrcl} m_x\ddot{r}_x & - & \frac{m_3 l}{2}\sin(\theta)\ddot{\theta} & - & \frac{m_3 l}{2}\cos(\theta)\dot{\theta}^2 & = & k_m i_Y \\ m_y\ddot{r}_y & + & m_3 l\cos(\theta)\ddot{\theta} & - & m_3 l\sin(\theta)\dot{\theta}^2 & = & -k_m i_X \\ I\ddot{\theta} & - & m_3 l\sin(\theta)\ddot{r}_x & + & m_3 l\cos(\theta)\ddot{r}_y & = & -c_s\frac{2}{\pi}\arctan(\varphi\dot{\theta}) - c_v\dot{\theta} \end{array} \tag{3.2}$$

Here, the masses are given by

$$\begin{array}{rcl} m_x & = & \frac{m_{Y_1}+m_{Y_2}}{2} + \frac{m_B}{2} + \frac{m_X+m_3}{2} \\ m_y & = & m_X + m_3 \\ I & = & I_3 + m_3 l^2 \end{array} \tag{3.3}$$

The friction present in the link bearing has been modelled with a combination of Coulomb and viscous friction. The Coulomb friction is approximated using an arctangens function. The linearization of the above system is not controllable. In Appendix B, the controllability properties of the linearization of a model including horizontal tilt motion are investigated.

3.2 Derivation of IO control law

To apply IO linearization, the state space notation must be used. The state variables will be defined as:

$$\begin{array}{lllllllll} x_1 & = & r_x & & x_2 & = & r_y & & x_3 & = & \theta \\ x_4 & = & \dot{r}_x & , & x_5 & = & \dot{r}_y & , & x_6 & = & \dot{\theta} \end{array} \tag{3.4}$$

The state space representation of the equations of motion is quite complex. Therefore, merely the general structure will be given here:

$$\begin{bmatrix} \dot{x}_1 \\ \dot{x}_2 \\ \dot{x}_3 \\ \dot{x}_4 \\ \dot{x}_5 \\ \dot{x}_6 \end{bmatrix} = \begin{bmatrix} x_4 \\ x_5 \\ x_6 \\ f_4(x_3, x_6) \\ f_5(x_3, x_6) \\ f_6(x_3, x_6) \end{bmatrix} + \begin{bmatrix} 0 & 0 \\ 0 & 0 \\ 0 & 0 \\ g_{41}(x_3, x_6) & g_{42}(x_3, x_6) \\ g_{51}(x_3, x_6) & g_{52}(x_3, x_6) \\ g_{61}(x_3, x_6) & g_{62}(x_3, x_6) \end{bmatrix} \cdot \begin{bmatrix} i_Y \\ i_X \end{bmatrix} \tag{3.5}$$

From (3.5), the possible benefits of IO linearization directly come apparent. Due to the presence of the link, the lower half of both the drift term and the input term of the state space representation are strongly nonlinear. In addition, the inputs and outputs are coupled. The time-derivative of x_4 is influenced by both i_X and i_Y, the same applies to the time-derivative of x_5. With that, the link limits the performance of the H-drive as a servo system.

The actuated degrees of freedom are chosen as output functions, i.e.

$$y_1 = h_1(x) = x_1 \quad , \quad y_2 = h_2(x) = x_2 \tag{3.6}$$

In conformity with the theory from chapter 2, the derivation of the IO control law starts with determining the Lie derivatives of y_1 and y_2.

$$\begin{array}{lllllllll} L_f h_1(x) & = & x_4 & & L_g h_1(x) & = & 0 \\ L_f h_2(x) & = & x_5 & , & L_g h_2(x) & = & 0 \end{array} \tag{3.7}$$

Because no inputs appear in the first Lie derivatives, the second Lie derivatives are computed:

$$\begin{aligned} L_f^2 h_1(x) &= \frac{m_3 l \cos(x_3) x_6^2 \left(m_y I - m_3 l\right) - m_y \sin(x_3) \left(c_v x_6 + c_s \frac{2}{\pi} \arctan(\varphi x_6)\right)}{D(x)} \\ L_g L_f h_1(x) &= \frac{\left(m_y I - m_3^2 l^2 \cos(x_3^2)\right) k_m}{D(x)} i_Y + \frac{\left(m_3^2 l^2 \cos(x_3) sin(x_3)\right) k_m}{D(x)} i_X \\ L_f^2 h_2(x) &= \frac{m_3 l \sin(x_3) x_6^2 \left(2 m_x I - m_3 l\right) + m_x \cos(x_3) \left(c_v x_6 + c_s \frac{2}{\pi} \arctan(\varphi x_6)\right)}{D(x)} \\ L_g L_f h_2(x) &= \frac{-2 m_3^2 l^2 \cos(x_3) \sin(x_3) k_m}{D(x)} i_Y + \frac{\left(2 m_x I + \left(\cos(x_3^2) - 1\right) m_3^2 l^2\right) k_m}{D(x)} i_X \end{aligned} \tag{3.8}$$

The denominator $D(x)$ which appears in the foregoing expressions is given by:

$$D(x) = 2m_x m_y I - 2m_3^2 l^2 m_y + m_3^2 l^2 \cos(x_3^2)(m_y - 2m_x) \tag{3.9}$$

Considering (3.8), both y_1 and y_2 have relative degree two. For both output functions the relative degree is well defined, i.e. $L_f L_g h_i(x) \neq 0 \quad \forall \quad x$ for $i = 1, 2$. The output functions chosen therefore serve as an appropriate basis for IO linearization. However, the numbers of inputs that appear in $L_g L_f h_1(x)$ and $L_g L_f h_2(x)$ do depend on x. For $x_3 = \frac{\pi}{2}$, $L_g L_f h_1(x)$ does not depend on i_X. This situation coincides with the link being parallel to the X axes. Owing to this i_X exerts no torque on the link. As a consequence, y_1 is not influenced by i_X. For $x_3 = 0$, $L_g L_f h_2(x)$ is independent of i_Y. In this case, the link is parallel to the Y axis and no torque is exerted on the link by i_Y. Therefore, y_2 will not be influenced by i_Y in that case.

Next, an IO linearizing control law u is computed using (2.7). An expression for u is:

$$\begin{bmatrix} i_Y \\ i_X \end{bmatrix} = \frac{1}{k_m}\Bigg(\begin{bmatrix} m_x \nu_x & + & \frac{m_3 l \sin(x_3)}{2I}\left(c_v x_6 + c_s \frac{2}{\pi}\arctan(\varphi x_6)\right) \\ \underbrace{m_y \nu_y}_{feed\ forward} & + & \underbrace{\frac{m_3 l \cos(x_3)}{I}\left(c_v x_6 + c_s \frac{2}{\pi}\arctan(\varphi x_6)\right)}_{tangential\ force\ due\ to\ friction} \end{bmatrix}$$

$$+ \begin{bmatrix} -\frac{m_3 l}{2}\cos(x_3) x_6^2 & - & \frac{m_3^2 l^2}{2I}\left(\sin^2(x_6)\nu_x + \sin(x_3)\cos(x_3)\nu_y\right) \\ \underbrace{m_3 l \sin(x_3) x_6^2}_{normal\ force} & - & \underbrace{\frac{m_3^2 l^2}{I}\left(\sin(x_3)\cos(x_3)\nu_x - \cos^2(x_3)\nu_y\right)}_{tangential\ force\ due\ to\ inputs} \end{bmatrix} \Bigg) \tag{3.10}$$

The control law presented above, is a combination of rigid body feedforward and an exact cancellation of the normal and tangential forces exerted by the link using a computed torque control law. The additional controllers ν_x and ν_y are chosen the following way:

$$\begin{aligned} \nu_x &= \ddot{y}_{1_{ref}} - k_0 \dot{e} - k_1 e \\ \nu_y &= \ddot{y}_{2_{ref}} - k_0 \dot{e} - k_1 e \end{aligned} \tag{3.11}$$

The coefficients k_0 and k_1 are to be chosen such that ν_x and ν_y are Hurwitz. By doing so, the input output behavior will be globally asymptotically stabilized.

In theory, IO linearization does not require an additional servo system to control the H-drive. In practice however, the servo controllers mentioned in section 3.1 will be employed when IO linearization is implemented. The servo controllers are required for two reasons. First, tilt of the X-beam is to be prevented. Since tilt is not accounted for in the equations of motion, the servo controllers are necessary to ensure that $Y_1(t) = Y_2(t) \quad \forall \quad t$. Second, the servo controllers are able to compensate or suppress unmodelled dynamics and unknown disturbances such as friction and cogging.

The control structure consisting of a high level nonlinear controller and a low level servo controller is often referred to as "virtual internal model following control", see [1] and [3]. Figure 3.2 shows the control structure implemented. The servo controllers for

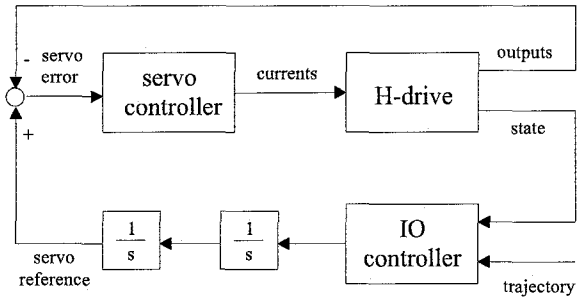

Figure 3.2: Control structure implemted on the underactuated H-drive. The H-drive is controlled by a combination of a high level IO controller and a low level servo controller. The output of the high level controller is integrated twice in order to obtain a reference to follow by the low level controller.

X and Y are of equal structure, both are of the type PI lead/lag. Since the masses associated with motions along the X- and Y-direction are different, the servo controllers for X and Y differ in gain. The tuning of the low level servo controllers is discussed more detailed in [1].

From itself, IO linearization has very poor robustness properties since it relies on exact cancellation of nonlinearities. The robustness of IO linearization w.r.t. parameter uncertainties, unmodelled dynamics and disturbances will be largely increased when an additional servo system is applied. Given an imperfect model, the virtual internal model following control approach might prove indispensable for a useful application of IO linearization.

Essentially, the use of an additional linear servo controller does not alter the input output behaviour from being linear. However, the presence of a servo error will disturb the linearity of the input output behaviour. As a consequence, no exact IO linearization will be obtained when a servo error is present. The smaller the servo error, the more the benefits of IO linearization will be attained. The servo error acts as a lower bound on the tracking error; the tracking error will in no case be smaller than the servo error. Concluding: the servo controller should be designed such that the servo error is minimized. Then, the benefits of IO linearization are attained maximally.

3.3 Tracking and zero dynamics

In order to evaluate the zero and tracking dynamics of the underactuated H-drive, the transformation to the normal form is employed. The first four coordinates are chosen

in conformity with (2.11):

$$\begin{array}{lllll} z_1 & = & h_1(x) & = & x_1 \\ z_2 & = & L_f h_1(x) & = & x_4 \\ z_3 & = & h_2(x) & = & x_2 \\ z_4 & = & L_f h_2(x) & = & x_5 \end{array} \tag{3.12}$$

The remaining coordinates z_5 and z_6 are chosen such that the transformation to the normal form is regular. The simplest way to make the transformation regular is choosing $z_5 = x_3$ and $z_6 = x_6$. In that case the transformation is one to one; the Jacobian of z w.r.t. x will have full rank. The dynamics in the normal form are consequently:

$$\begin{array}{lll} \dot{z}_1 & = & z_2 \\ \dot{z}_2 & = & \nu_x \\ \dot{z}_3 & = & z_4 \\ \dot{z}_4 & = & \nu_y \\ \dot{z}_5 & = & z_6 \\ \dot{z}_6 & = & \frac{-c_v z_6 - c_s \frac{2}{\pi} \arctan(\varphi z_6) + m_3 l \sin(z_5)\nu_x - m_3 l \cos(z_5)\nu_y}{I} \end{array} \tag{3.13}$$

The dynamics in normal form clearly shows that z_1 and z_3 (x_1 and x_2) are decoupled w.r.t. to the inputs. Moreover, they are decoupled from the disturbing effects of the rotating link. Furthermore, the dynamics in z_5 and z_6 do not depend on z_1 up to z_4. The tracking dynamics are obtained from (3.13) by assuming the tracking error has vanished. In that case, no dynamics are present in the coordinates z_1 up to z_4. By doing so, the tracking dynamics are:

$$\begin{array}{lll} \dot{z}_5 & = & z_6 \\ \dot{z}_6 & = & \frac{-c_v z_6 - c_s \frac{2}{\pi} \arctan(\varphi z_6) + m_3 l \sin(z_5)\ddot{z}_{1_{ref}} - m_3 l \cos(z_5)\ddot{z}_{3_{ref}}}{I} \end{array} \tag{3.14}$$

The tracking dynamics coincide with the link's motion that arises when z_1 and z_3 are forced to track a certain reference. Expression (3.14) merely states that the angular acceleration is influenced by the torque of $\ddot{z}_{1_{ref}}$ and $\ddot{z}_{3_{ref}}$ and by the friction present in the bearing. The stability of the tracking dynamics depends on the specific trajectories imposed on z_1 and z_3. Using the Jacobian linearization of (3.14), this dependency will be (locally) investigated. Assuming $\ddot{z}_{1_{ref}} =$ constant and $\ddot{z}_{3_{ref}} = 0$, the linearization of (3.14) around the origin of (z_5, z_6) is:

$$\begin{bmatrix} \dot{z}_5 \\ \dot{z}_6 \end{bmatrix} = \begin{bmatrix} 0 & 1 \\ \frac{m_3 l \ddot{z}_{1_{ref}}}{I} & \frac{-c_v - c_s \frac{2}{\pi}\varphi}{I} \end{bmatrix} \begin{bmatrix} z_5 \\ z_6 \end{bmatrix} \tag{3.15}$$

The parameters c_v, c_s and φ are positive. Due to the friction terms present in A_{22}, one of the eigenvalues of A will have negative real part. The second eigenvalue can have negative or positive real part depending on the value of $\ddot{z}_{1_{ref}}$.

If $\ddot{z}_{1_{ref}}$ is negative, the second eigenvalue will have negative real part. In that case, the tracking dynamics are asymptotically stable. Given nonzero initial conditions, the link

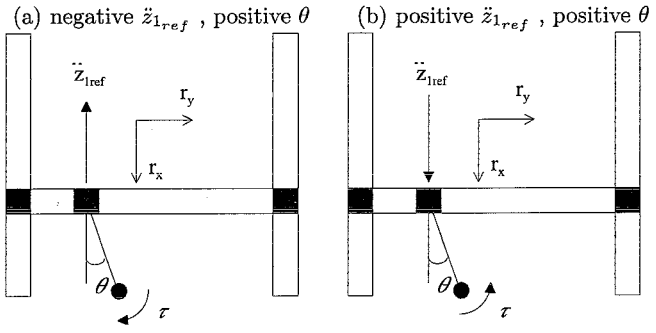

Figure 3.3: Dependence of the local stability on the sign of the reference trajectory imposed

will be stabilized in the origin by a torque τ which is caused by $\ddot{z}_{1_{ref}}$. Figure 3.3 (a) shows the initial orientation of the link and the accompanying torque in case of negative $\ddot{z}_{1_{ref}}$.

If $\ddot{z}_{1_{ref}}$ is positive, the second eigenvalue will have positive real part. Thereby, the tracking dynamics will be unstable. Assuming nonzero initial conditions, the link will be stabilized in $(z_5, z_6)=(\frac{\pi}{2}, 0)$ by a torque τ caused by $\ddot{z}_{1_{ref}}$. Figure 3.3 (b) shows the initial orientation of the link and the accompanying torque in case of positive $\ddot{z}_{1_{ref}}$. Note that the stability properties of the tracking dynamics as derived are only valid in case of constant $\ddot{z}_{1_{ref}}$.

The zero dynamics are obtained from (3.14) by setting $\ddot{z}_{1_{ref}}$ and $\ddot{z}_{3_{ref}}$ equal to zero. The zero dynamics of the underactuated H-drive are:

$$\begin{aligned} \dot{z}_5 &= z_6 \\ \dot{z}_6 &= -\frac{c_v z_6 + c_s \frac{2}{\pi} \arctan(\varphi z_6)}{I} \end{aligned} \tag{3.16}$$

The zero dynamics coincide with the link's freedom to rotate when the control goals for z_1 and z_3 have been achieved. The stability of the zero dynamics can not be investigated using the Jacobian linearization of (3.16). The Jacobian linearization is inconclusive about stability because it has a zero eigenvalue. Therefore, the stability properties of the zero dynamics will be investigated by analyzing (3.16) directly.

The second equation of (3.16) is independent of z_5. From this equation, one can directly observe that z_6 (the angular velocity of the link) will decay to zero; the equilibrium point $z_6 = 0$ is asymptotically stable. However, z_6 will decay to zero for whatever value of z_5. As a consequence, a continuum of equilibrium points is present in case of z_5. Physically, the characteristics of the zero dynamics can be understood by the fact that the link will decelerate due to friction and finally come at rest at some arbitrary position.

Chapter 4

Simulations and experiments

In order to evaluate the performance of the control strategy implemented, simulations and experiments have been conducted. First, results in case of constant tracking will be discussed. Hereafter, results obtained with a periodic reference trajectory are discussed.

The values for the parameters in the simulations and experiments are chosen in agreement with the values obtained by the least squares identification procedure performed in [1]. Results of this procedure are given in table 4.1. Because φ is parameterized nonlinearly in (3.2), it is not identified by the least squares procedure. Therefore, a rough estimate for φ is used. The values for k_0 and k_1 are chosen such that the eigenvalues of the error dynamics equal -50. Physical limitations of the H-drive restrict the eigenvalues to this level.

4.1 Constant tracking

Because of the H-drive's physical limitations, instead of a step function, a third order profile is used as a reference trajectory for constant tracking. Since the third order profile is more smooth, it requires much smaller accelerations than a step profile.

On both outputs y_1 and y_2, the same third order profile is imposed. The initial conditions x_0 are $[0.2, 0.2, 0, 0, 0, 0]$. Figure 4.1 shows the state variables for both simulation and experiment. In case of x_1, x_2 and the accompanying time-derivatives, simulation and experimental results agree well. Therefore, the control structure implemented is robust to unmodelled phenomena indeed. Overshoot w.r.t. to the third order profile can be observed.

Simulation and experimental results differ in case of the link motion. The simulation predicts a larger angular velocity just after the start of the third order profile. Reason for the difference observed might be the approximation of Coulomb friction with an arctangent function; this approximation underestimates the effects of static friction.

Table 4.1: simulation parameters

parameter	value	unit
k_m	74.4	[N/A]
m_x	$0.21914 \cdot k_m$	[kg]
m_y	$0.14066 \cdot k_m$	[kg]
m_3	0.04	[kg]
I	8e-4	[kgm^2]
L	0.15	[m]
c_s	$0.3320 \cdot I$	[Ns/m]
c_v	$0.0217 \cdot I$	[N]
φ	100	[s]
k_0	100	[1/s]
k_1	2500	[1/s^2]

After the third order profile attains a constant value, the motion of the link can be viewed as the zero dynamics of the underactuated H-drive. The angular velocity x_6 decays to zero. The angle x_3 takes an arbitrary value. The zero dynamics behave as derived in section 3.3.

The tracking errors are shown in the upper plots of figure 4.2. The error dynamics for y_1 and y_2 are qualitatively equal. The explanation for the mutual differences is twofold. First, the references generated by the integrators differ, see figure 3.2. Second, the servo controllers differ in gain. The peak values of the tracking errors coincide with the overshoot in x_1 and x_2. Vibrational behavior can be observed in the tracking error after the third order profile attains a constant value, see the middle plots of figure 4.1 which provide an enlarged view.

The vibration in the tracking error is caused by forces exerted by the rotating link. The amplitude of the vibration is approximately related to the square of the angular velocity, i.e. it is related to the centrifugal force. The frequency is directly proportional to the angular velocity. Because the angular velocity decreases due to friction, both the vibration's amplitude and frequency decay with time. The effects of the rotating link are significantly smaller in case of the experiment. The explanation for this is given by the fact that the angular velocity measured is smaller. In addition, friction on the axes of the H-drive (which has not been accounted for in the simulations), will diminish the disturbing effects of the rotating link. The fact that rotation of the link affects the tracking error indicates that no exact IO linearization is obtained.

The currents are shown in the lower plots of figure 4.2. In case of the simulation, the currents are proportional to the tracking errors. The currents measured in the experiment can be related less evidently to the tracking errors. The currents measured are substantially larger due to unmodelled phenomena such as friction, cogging and measurement noise.

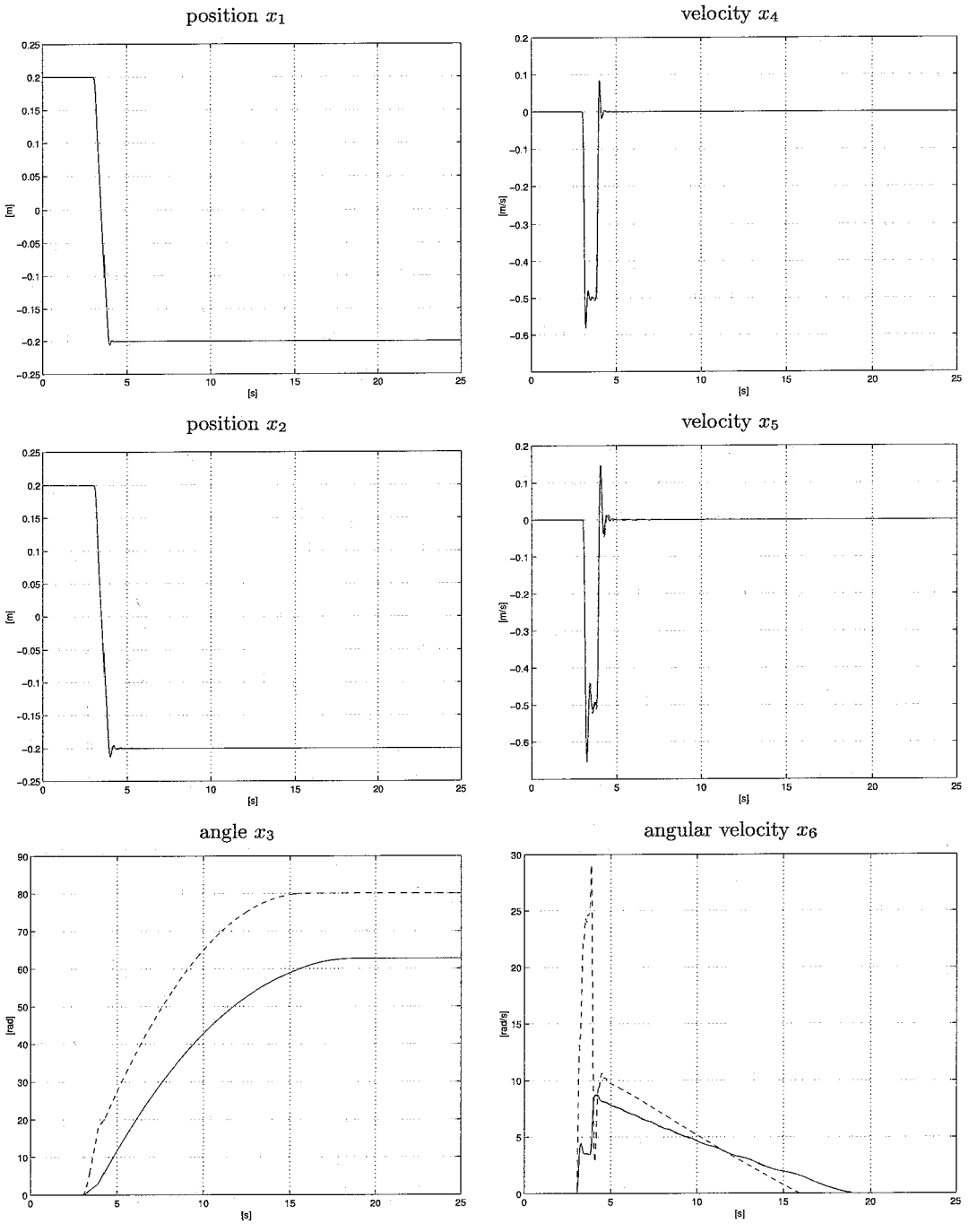

Figure 4.1: State variables constant tracking. Reference trajectories for x_1 and x_2: dotted. Simulation results: dashed. Experimental results: solid

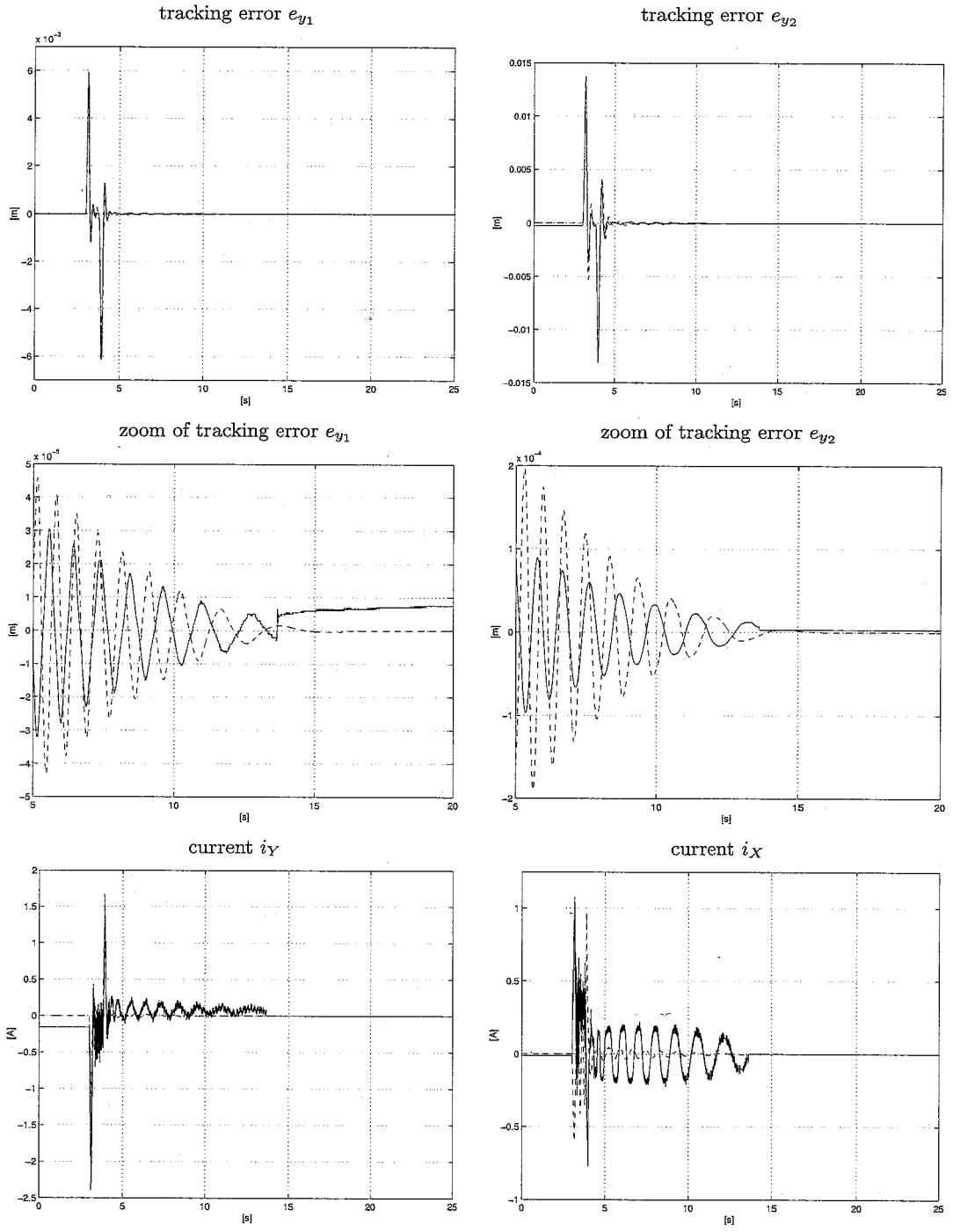

Figure 4.2: Errors and currents constant tracking. Simulation results: dashed. Experimental results: solid

4.2 Periodic tracking

Periodic trajectories have been specified for the outputs y_1 and y_2, they are respectively given by:

$$\begin{aligned} y_{1_{ref}} &= 0.2\sin(2\pi 0.25t) \\ y_{2_{ref}} &= 0.2\cos(2\pi 0.25t) \end{aligned} \tag{4.1}$$

Imposing the trajectories defined in (4.1), a uniform circular motion in the horizontal plane is obtained. The initial conditions x_0 are $[0.16\ ,\ 0.24\ ,\ \frac{\pi}{2}\ ,\ 0\ ,\ 0\ ,\ 0]$. The state variables are shown in figure 4.1. As can be seen, the initial conditions for x_1 and x_2 do not coincide with the initial values of the reference trajectories. This mismatch has been introduced to obtain more transient behavior. Like the stabilization experiment, simulation and experimental results agree very well for coordinates x_1, x_2 and their time-derivatives.

The lower plots in figure 4.3 show the orientation and the angular velocity of the link. As can be seen, the angular velocity approaches a constant value. The uniform circular motion has constant normal acceleration and zero tangential acceleration. In this way, a constant torque is exerted on the link. This torque will finally balance with the friction torque acting on the link. As a consequence, the angular velocity will take a value of $2 \cdot \pi \cdot 0.25\ \frac{rad}{s}$ which is equal to the angular frequency of the trajectories imposed. The angle of the link will increase approximately linearly with time as figure 4.3 shows. For the reference trajectories given by 4.1, the link moves away from the origin. Consequently, the tracking dynamics are unstable. Again, simulation predicts a considerably larger angular velocity.

The tracking errors are shown in the upper plots of figure 4.4. Again, the errors e_{y_1} and e_{y_2} are qualitatively equal. Due to the mismatch of initial conditions, the tracking errors are quite large initially. After the transient has vanished, the errors show oscillatory behavior. In case of the simulation, a small vibration originating from the rotating link is superimposed on the tracking error. Due to the mismatch of initial conditions, simulation predicts a relatively high angular velocity initially. Next, friction decelerates the link. When the angular velocity has decayed to some small value, the link no longer affects the tracking error noticeably. In case of the experiment, no effects of the rotating link on the tracking error can be observed.

The currents are depicted in the lower plots of figure 4.4. In case of the simulation, the currents can be directly related to the tracking error. First, due to the mismatch of initial conditions, large currents are required to control the H-drive. The extraordinary large peak value of current i_Y is due to the abrupt transition caused by the nonzero initial time-derivative of the sine reference for y_1. Second, the IO linearizing control law aims at compensation of the effects of the rotating link; this is visible as a vibration superimposed on the current signal. Finally, the currents show oscillatory behavior. Again, the currents measured are considerably larger due to unmodelled phenomena such as friction, cogging and measurement noise. The oscillatory behavior of the tracking error can be recognized in the currents measured.

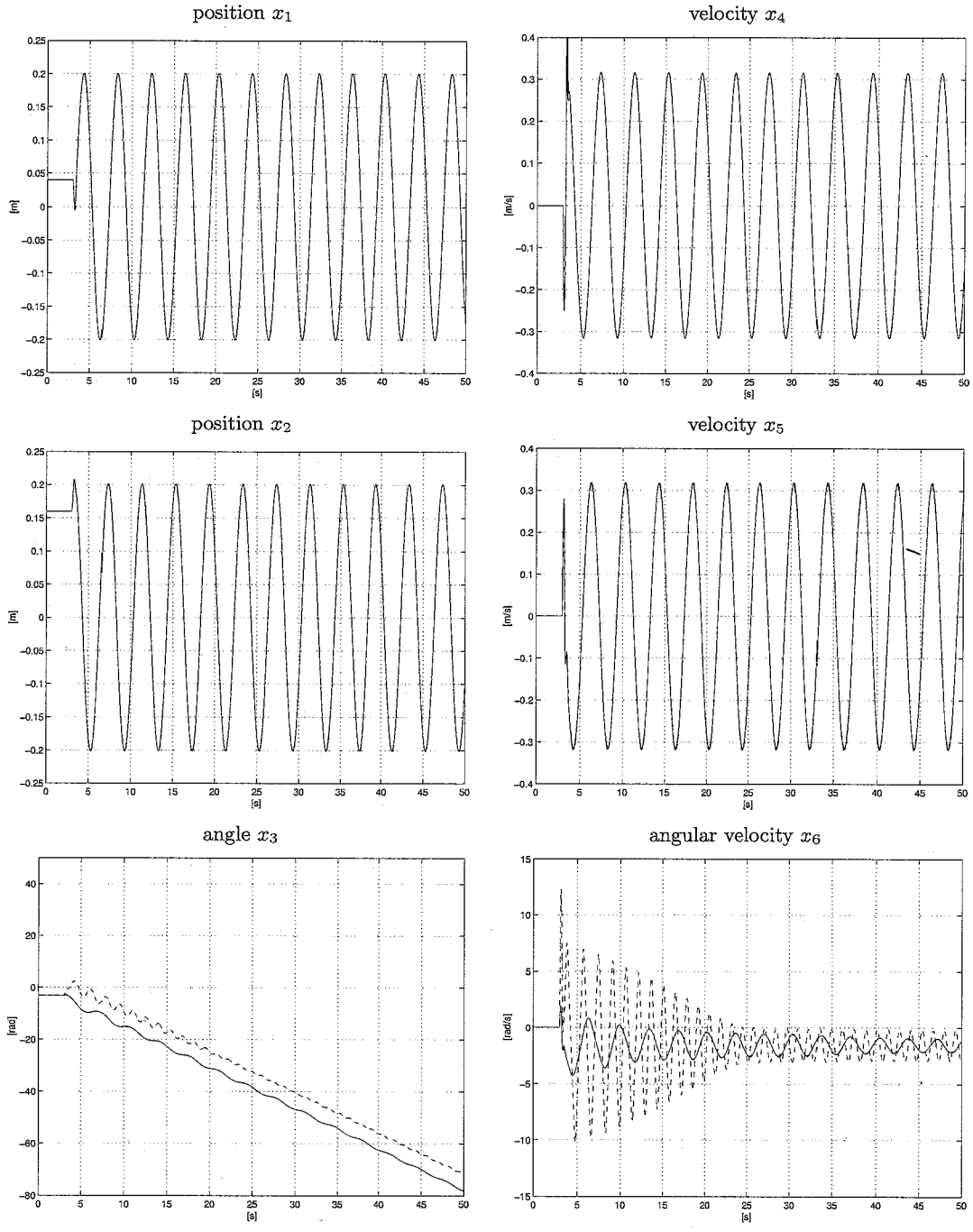

Figure 4.3: State variables periodic tracking. Reference trajectories for x_1 and x_2: dotted. Simulation results: dashed. Experimental results: solid.

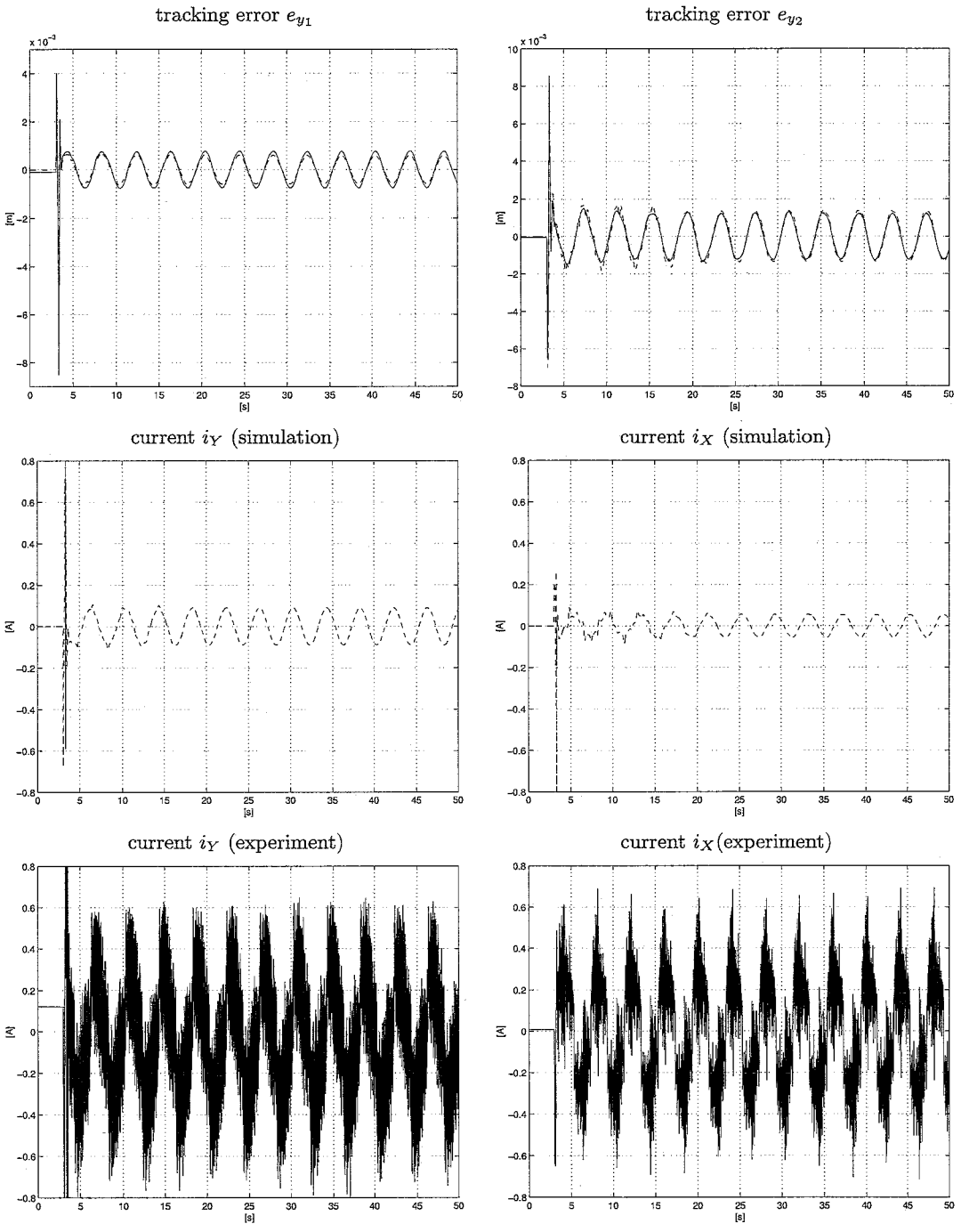

Figure 4.4: Errors and currents periodic tracking. Reference trajectory for x_1 and x_2: dotted. Simulation results: dashed. Experimental results: solid. The currents measured are displayed separately for the sake of clearness.

Chapter 5

Conclusions and recommendations

Conclusions

IO linearization is successfully implemented on the underactuated H-drive. The H-drive proves to be a system that is very suitable for the application of IO linearization.

The controlled DOFs of the H-drive are globally stabilized using linear pole placement techniques.

Using the virtual internal model following control approach, a robust form of IO linearization is obtained. Given an imperfect model and the presence of disturbances, this strategy may be indispensable for a useful application of IO linearization.

Simulation and experimental results agree wel for the actuated DOFs. In case of the link, simulation predicts larger angular velocities. This may be due to the approximation of static friction with an arctangent function.

No exact IO linearization is obtained. Reason for this is the inability of the additional servo controller to exactly track the compensation generated by the IO linearizing controller.

Recommendations

As mentioned no exact IO linearization is employed due to the presence of the low level servo controller. To start off with, future research should be dedicated to the tuning of the servo controller in order to obtain a smaller servo error. Likely, feedforward can decrease the servo error.

Secondly, the need for the low level servo controller must be removed. In order to do so, a more accurate model for the H-drive must be derived. The horizontal tilt motion of the X-beam must be accounted for in this model. It must also include a suitable friction model for friction on the X an Y axes.

Finally, one should include flexibilities in the model in order to make the strategy possible for high frequent application. Because a relatively simple rigid body model has been used till so far, results obtained are only valid low frequent (i.e. below the first resonance frequency of the H-drive).

Bibliography

[1] N.P.I. Aneke. *Control of underactuated mechanical systems.* PhD thesis, Technische Universiteit Eindhoven, 2003.

[2] H. Arai. *Nonholonomic control of three-dof planar underactuated manipulator.* 1998. IEEE transactions on Robotics and automation, volume 14, pp. 681 - 695.

[3] K. Kosuge. *Virtual internal model following control of robot arms.* 1987. Proceedings of the IEEE international conference on Robotics and automation, volume 1, pp. 1549 - 1554.

[4] S. Sastry. *Nonlinear systems - Analysis, stability and control.* Springer Verlag, New York, 1999.

Appendix A

Evaluation of the experimental setup

A.1 Introduction

Using the chained from controller designed in [1] it is possible to control the three degrees of freedom of the H-drive using only two inputs. A top view of the H-drive is given in figure A.1. The positions of the Y-sleds $Y1$ and $Y2$ are kept equal to prevent misalignment of the X-sled.

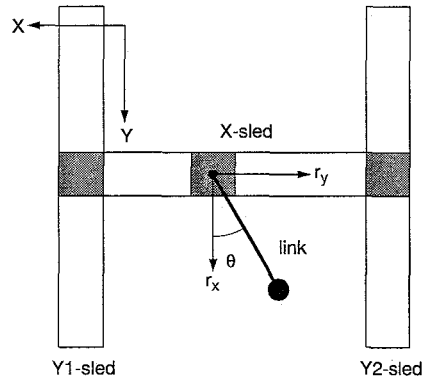

Figure A.1: Top view of the H-drive with three independent sleds X, $Y1$ and $Y2$. The machine coordinates (X, Y) have their origin in the top-left corner. The origin of the link coordinates (r_x, r_y, θ) is placed in the middle of the H-drive with the link facing downwards.

When conducting stabilization experiments on the H-drive, several problems arise due to perturbations. The main perturbations are assumed to be gravitational forces and friction in the bearing of the link. The expected effect of the perturbations is preferential

Table A.1: Gains of the chained form controller.

gain	k_1	k_2	k_3	k_4	k_5	k_6	ϵ
value	4	$2\sqrt{2}$	15	15	9	6	0.25

behavior of the experimental setup, i.e. an asymptotically stable equilibrium position for the link is being introduced. If the link would rotate in a plane which is aligned exactly perpendicular to gravity, no asymptotically stable equilibrium point would exist. If the link was actuated, perturbations could be suppressed for. However, since the link is not actuated, perturbations can strongly influence the motion of the link.

The gravitational torque is caused by a misalignment of the plane of rotation of the link with the horizontal plane. This misalignment has two sources: the platform in which the bearings are held can be misaligned and in addition the bearings guiding the axis might not be mounted perpendicular to the platform. Unfortunately, at the moment there is no way to measure the tilt of the axis directly. Merely the misalignment of the platform can be measured. Measurements are carried out using a very basic spirit level[1].

In this chapter, a range of stabilization experiments is discussed. The aim of these experiments is to investigate the influence of the perturbations mentioned and the possibilities of compensating them. For all measurements, unless indicated otherwise, the reference position for the controller is the origin of the (r_x, r_y) coordinate system, the angle $\theta = 0$ and all velocities equal to zero. The gains of the chained form controller as stated in table A.1 are the same as used in [1]. In order to obtain practical convergence when using the chained form controller, the motors are switched off when the error between the actual state and the desired state is smaller than some threshold α, i.e.:

$$|x(t) - x_d| \leq \alpha \tag{A.1}$$

Without using this convergence criterion, a sustaining response around the reference position would result. For more information on the practical convergence condition, see [1]. The remaining error of the link angle will be investigated. This quantity is a measure for the preferred behavior. The remaining error is defined as the error that remains when the practical convergence conditions are met and the system is at rest, see [1]. The errors in r_x and r_y direction are given as additional information but will not be discussed. Possible asymmetry of the experimental setup is investigated using two different initial positions. These initial positions are mirrored w.r.t. the Y-axis, see figure A.2.

[1] a spirit level = een waterpas

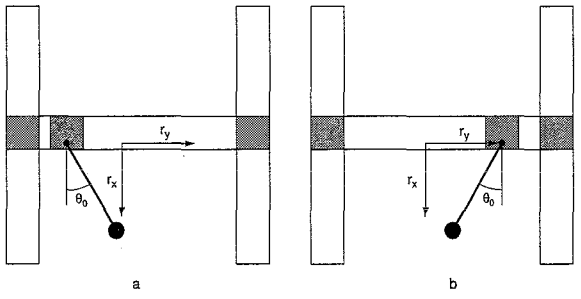

Figure A.2: Start position of link with positive initial angle θ_0 (a) and with negative θ_0 (b).

A.2 Experiments using a levelled platform

The aim of the experiments described in this section is to explore the characteristics of the experimental setup with a levelled platform. Assuming the axis is mounted perpendicular onto the platform no influence of gravitational torque is to be expected. In that case, the mean remaining error of θ should be zero for both initial positions.

In figure A.3 an experiment is shown using a positive initial angle. The remaining errors for all measurements with both positive and negative initial angles are given in tables A.2 and A.3. Unfortunately, the number of experiments differ for the two initial angles. After changing the orientation of the platform recreating an experimental setup is not possible and thus no extra measurements could be performed afterwards.

The remaining errors in θ suggest that the axis of the link is tilted because the mean remaining error is smaller than zero for both positive and negative initial positions. The discrepancy in the mean error in case of positive and negative initial positions might be caused by the asymmetric friction in the bearing. The next set of measurements is focussed on eliminating the gravitational torque.

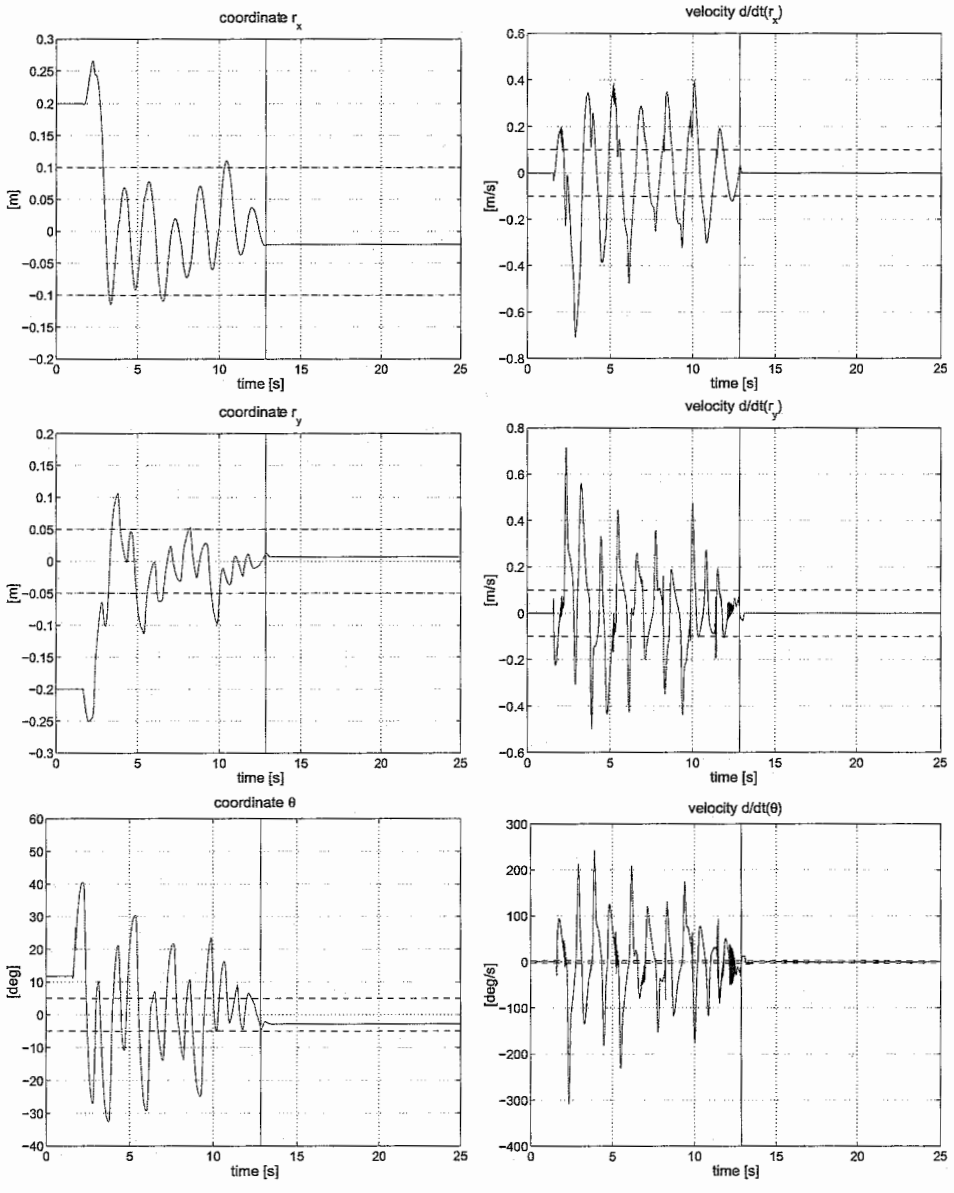

Figure A.3: Single measurement with levelled platform, positive initial angle and 0° reference angle.

Table A.2: Remaining error in r_x, r_y and θ for experiments with the levelled platform, 0° reference angle and negative initial position. The average error μ and standard deviation σ are calculated for these experiments.

measurement	$r_x - r_{x,d}$ [cm]	$r_y - r_{y,d}$ [cm]	$\theta - \theta_d$ [deg]
1	4.63	0.63	-3.00
2	0.41	-0.02	-1.17
3	-2.56	0.64	-2.53
4	-2.49	0.38	-1.11
5	-1.77	1.38	-4.55
6	-3.99	0.71	-5.67
7	-1.12	0.24	-0.67
8	-4.01	0.74	-4.14
μ	-1.36	0.59	-2.85
σ	2.83	0.42	1.82

Table A.3: Remaining error in r_x, r_y and θ for experiments with the levelled platform, 0° reference angle and positive initial position.

measurement	$r_x - r_{x,d}$ [cm]	$r_y - r_{y,d}$ [cm]	$\theta - \theta_d$ [deg]
1	4.33	-0.52	2.29
2	-1.11	0.23	-1.04
3	0.10	0.71	-3.79
4	-2.07	0.71	-2.84
5	-1.84	0.53	-1.75
6	-0.86	0.24	-0.83
7	5.97	-0.85	1.28
μ	0.65	0.15	-0.95
σ	3.19	0.61	2.15

A.3 Experiments with tilted platform

In order to compensate the gravitational torque caused by tilt of the axis, a misalignment of the platform with the horizontal plane has been applied. Based on the results with the levelled platform a small tilt around the Y-axis is applied lifting the left side of the platform and with that making the link's plane of rotation coincide with the horizontal plane, see figure A.4. The tilt is corrected heuristically, because no dedicated equipment

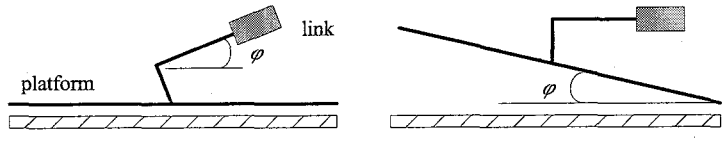

Figure A.4: The link is assumed to be tilted an angle φ, the platform is therefore tilted with the angle φ.

for measuring the tilt is available in the laboratory.

In figure A.5 a representative experiment is shown. For negative as well as positive initial angles, the mean remaining error in θ is decreased by the small misalignment of the platform, see tables A.4 and A.5. However, the benefit of the misalignment is limited: it seems only possible to shift the mean remaining error to zero for either positive or negative initial angles. The difference in the mean errors in θ observed in the experiments with a levelled platform, is still present. A possible explanation for this could be the presence of asymmetric friction in the bearings guiding the link.

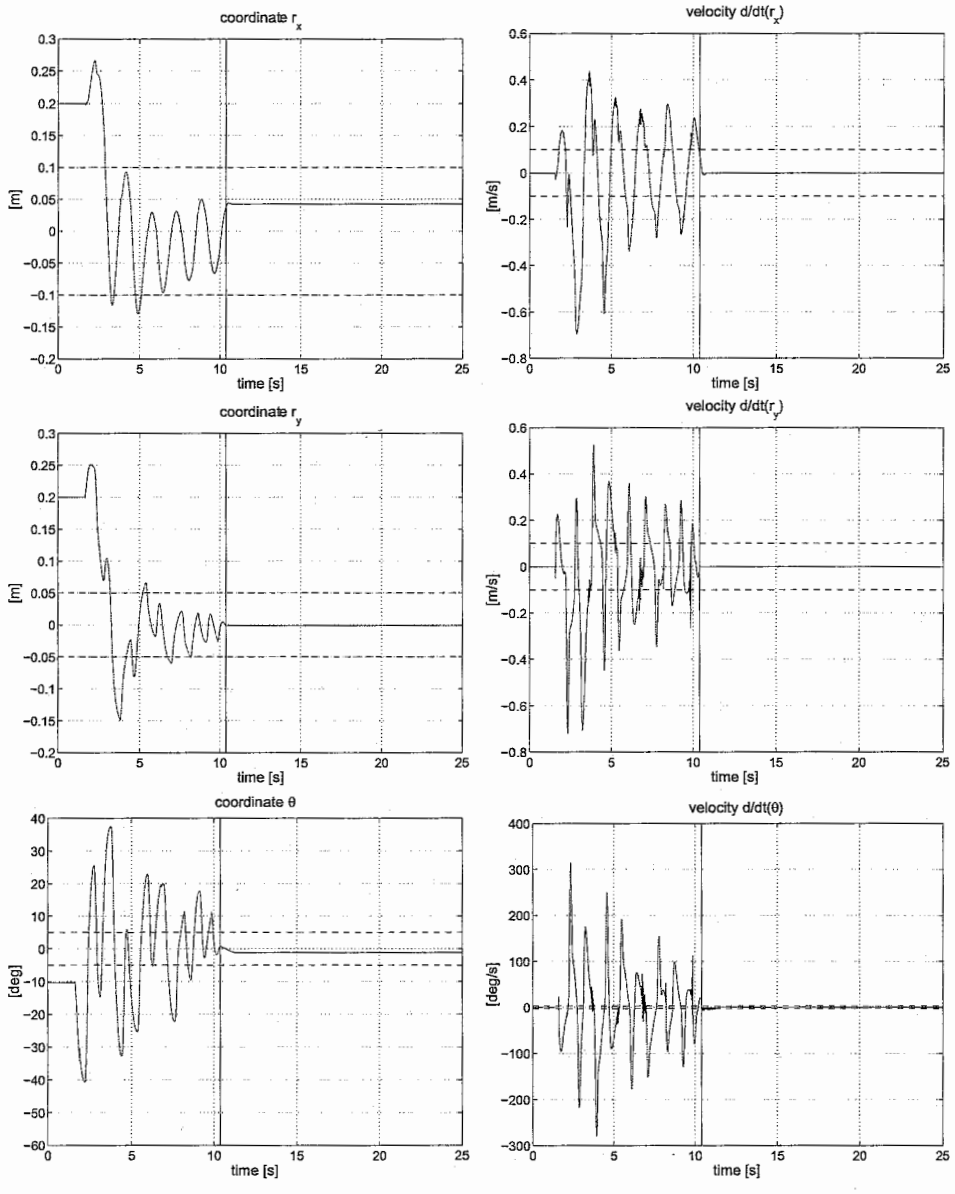

Figure A.5: Single measurement with tilted platform, negative initial angle and 0° reference angle.

Table A.4: Remaining error in r_x, r_y and θ for experiments with the tilted platform, 0° reference angle and negative initial position.

measurement	$r_x - r_{x,d}$ [cm]	$r_y - r_{y,d}$ [cm]	$\theta - \theta_d$ [deg]
1	3.98	-0.79	3.01
2	5.12	-0.50	-0.74
3	4.30	-0.69	0.95
4	0.03	-0.39	0.43
5	3.98	-0.20	-0.57
6	-2.60	-0.75	-1.83
7	4.27	-0.13	-1.18
8	1.47	0.15	-2.62
9	3.70	0.60	-4.80
10	4.07	0.61	-2.85
μ	2.83	-0.21	-1.02
σ	2.44	0.52	2.20

Table A.5: Remaining error in r_x, r_y and θ for experiments with the tilted platform, 0° reference angle and positive initial position.

measurement	$r_x - r_{x,d}$ [cm]	$r_y - r_{y,d}$ [cm]	$\theta - \theta_d$ [deg]
1	0.71	-0.15	0.18
2	3.92	-0.45	1.07
3	0.91	0.02	-1.58
4	-2.80	0.69	-3.81
5	0.65	0.07	0.48
6	0.87	-0.11	-0.18
7	0.89	-0.10	-0.31
8	4.15	-0.73	1.86
9	3.62	-1.18	4.44
10	0.67	-0.05	-0.67
μ	1.36	-0.20	0.15
σ	2.08	0.50	2.16

A.4 Stabilizing a different reference angle

In order to investigate the effects of asymmetric friction in the bearing guiding the link, the reference position for θ has been changed. Due to the limited dimensions of the H-drive, the maximum angle that can be stabilized equals about $\pm 5°$.

The response when $\theta_d = 5°$ and θ_0 positive is shown in figure A.6. The remaining errors for all combinations of the reference angle and the initial angle are shown in tables A.6, A.7, A.8 and A.9. For a reference angle of $-5°$ the mean remaining errors in θ are equal for both positive and negative initial angles and is negative. The variance is about 50% larger compared to experiments with a reference angle equal to zero. The experiments using $\theta_d = 5°$ show a different pattern. The variance is about equal to experiments with $\theta_d = 0°$ while the mean error is different for positive and negative initial angles.

The results above suggest preferred behavior is still present in the experimental setup. The tilt introduced to the platform has not exactly compensated the effects of gravitational torque. Therefore, an equilibrium position for the link different from zero is present. Considering the results above, the equilibrium position of the link must be just over 180°. As a consequence, the gravitational torque acting on the link is about zero when the reference angle equals 5°. In case of a reference angle of $-5°$, the gravitational torque pushes the link towards the equilibrium position. The explanation just stated could also explain the result that for most other reference angles the link is on the left side of its desired position.

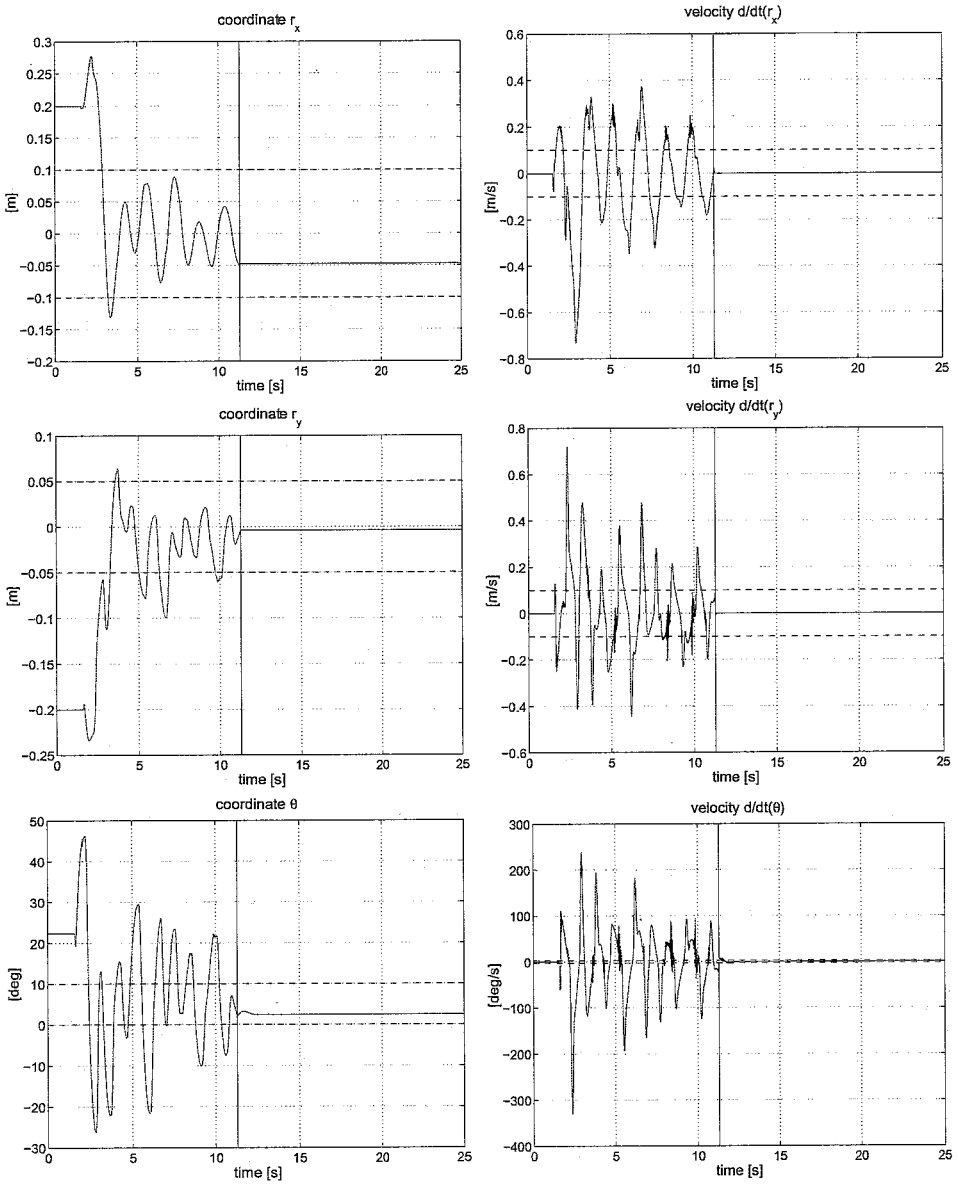

Figure A.6: Single measurement with tilted platform, positive initial angle and 5° reference angle.

Table A.6: Remaining error in r_x, r_y and θ for experiments with the tilted platform, $-5°$ reference angle and positive initial position.

measurement	$r_x - r_{x,d}$ [cm]	$r_y - r_{y,d}$ [cm]	$\theta - \theta_d$ [deg]
1	5.57	-0.77	-0.56
2	2.00	-1.27	2.43
3	2.15	0.37	-6.35
4	4.34	-1.31	3.27
5	5.30	-0.73	-0.38
6	4.19	0.35	-4.20
7	5.21	0.32	-2.93
8	-2.11	0.59	-2.84
9	4.09	-1.38	3.46
10	0.79	-0.26	-1.06
μ	3.15	-0.41	-0.92
σ	2.44	0.78	3.27

Table A.7: Remaining error in r_x, r_y and θ for experiments with the tilted platform, $-5°$ reference angle and negative initial position. The average error μ and standard deviation σ are calculated for these experiments.

measurement	$r_x - r_{x,d}$ [cm]	$r_y - r_{y,d}$ [cm]	$\theta - \theta_d$ [deg]
1	3.80	-1.62	4.18
2	4.67	-1.35	4.16
3	-4.00	1.58	-3.97
4	3.92	0.27	-4.37
5	0.64	0.72	-3.31
6	3.06	-0.72	1.66
7	-1.75	0.58	-2.07
8	-2.80	1.88	-5.18
9	4.06	-0.98	2.74
10	-2.36	1.37	-3.80
μ	0.92	0.17	-1.00
σ	3.36	1.27	3.75

Table A.8: Remaining error in r_x, r_y and θ for experiments with the tilted platform, 5° reference angle and positive initial position.

measurement	$r_x - r_{x,d}$ [cm]	$r_y - r_{y,d}$ [cm]	$\theta - \theta_d$ [deg]
1	0.46	0.20	-1.14
2	4.42	-0.21	1.13
3	0.83	0.09	-1.18
4	2.92	-1.94	4.50
5	4.22	0.10	-0.34
6	4.86	-0.37	1.60
7	-4.76	-0.38	-2.50
8	4.08	-0.65	4.31
9	0.69	0.17	-1.25
10	-3.20	-1.94	3.32
μ	1.45	-0.49	0.85
σ	3.32	0.81	2.52

Table A.9: Remaining error in r_x, r_y and θ for experiments with the tilted platform, 5° reference angle and negative initial position.

measurement	$r_x - r_{x,d}$ [cm]	$r_y - r_{y,d}$ [cm]	$\theta - \theta_d$ [deg]
1	4.76	-0.56	4.04
2	1.76	0.25	-2.71
3	3.18	0.26	-1.34
4	0.83	0.22	-1.48
5	0.67	0.04	-0.40
6	1.35	-0.19	-0.14
7	1.04	0.22	-1.33
8	1.30	0.11	-1.02
9	4.29	0.06	-0.10
10	0.97	-0.87	1.67
μ	2.01	-0.05	-0.28
σ	1.50	0.39	1.91

A.5 Experiments without using the practical convergence condition

Figure A.3 suggests convergence of θ to its desired value before the motors are switched off. The aim of the following experiments is to investigate whether the error is reduced by applying the control input for a longer period than the practical convergence condition would allow. Considering the foregoing experiments, practical convergence is obtained within 25 [s]. Therefor the response of the H-drive will be measured during a period of 50 [s] to be sure a steady state is achieved.

Figure A.7 shows the response of the state variables without using the practical convergence condition. The response observed in this specific experiment, is representative for all these experiments. A decreasing error can be observed until about 12 [s] (at that time the practical convergence conditions are met). After this time, a sort of periodic motion around the desired state arises. The amplitude of this oscillation does not decrease with time. The error will thus not be reduced by applying the input when the system ends up in its periodic motion.

If θ does convergence to its desired value without using the practical convergence condition, a reverse proportional relation between the time the practical convergence condition is satisfied and the remaining error could be expected. Figure A.8 shows the relation between the time the conditions for practical stabilization are met and the remaining error. There is no reverse proportional relation between the time of convergence and the remaining error in r_x, r_y or θ. The data featured in figure A.8 is representative for alle experiments, i.e. no experiment gives rise to the conclusion a relationship exists between the time needed for practical convergence and the remaining error.

The powerspectrum of the response after the conditions for practical convergence are met is shown in figure A.9. The powerspectra are calculated with a frequency resolution of 1/1024 Hz , using 512 samples overlap and the use of a Von Ham window. Possible aliasing effects can not be verified since no measurements are performed at higher sampling frequencies. In the chained form controller a time dependent term is used with frequency $\frac{2\pi}{\epsilon}$ Hz. The harmonics of this frequency are indicated in the figure. All three responses have a peak at about 85 Hz. This peak does not coincide with a harmonic of the frequency present in the control law. In r_y and θ a second peak can be seen at about 155 Hz. This frequency is not a multiple of the frequency present in the control law. This peak is not visible in the spectrum of r_x. Reason for this could be the fact that for $\theta \approx 0$, a movement in r_x direction does not influence the link. A harmonic analysis of the H-drive, conducted by R.Merrie, shows that the peak at 85 Hz as well as the peak at 155 Hz originate from resonances of the H-drive. The harmonic analysis of the response indicates that the periodic motion is not caused by the input; no harmonics of the input are present in the response.

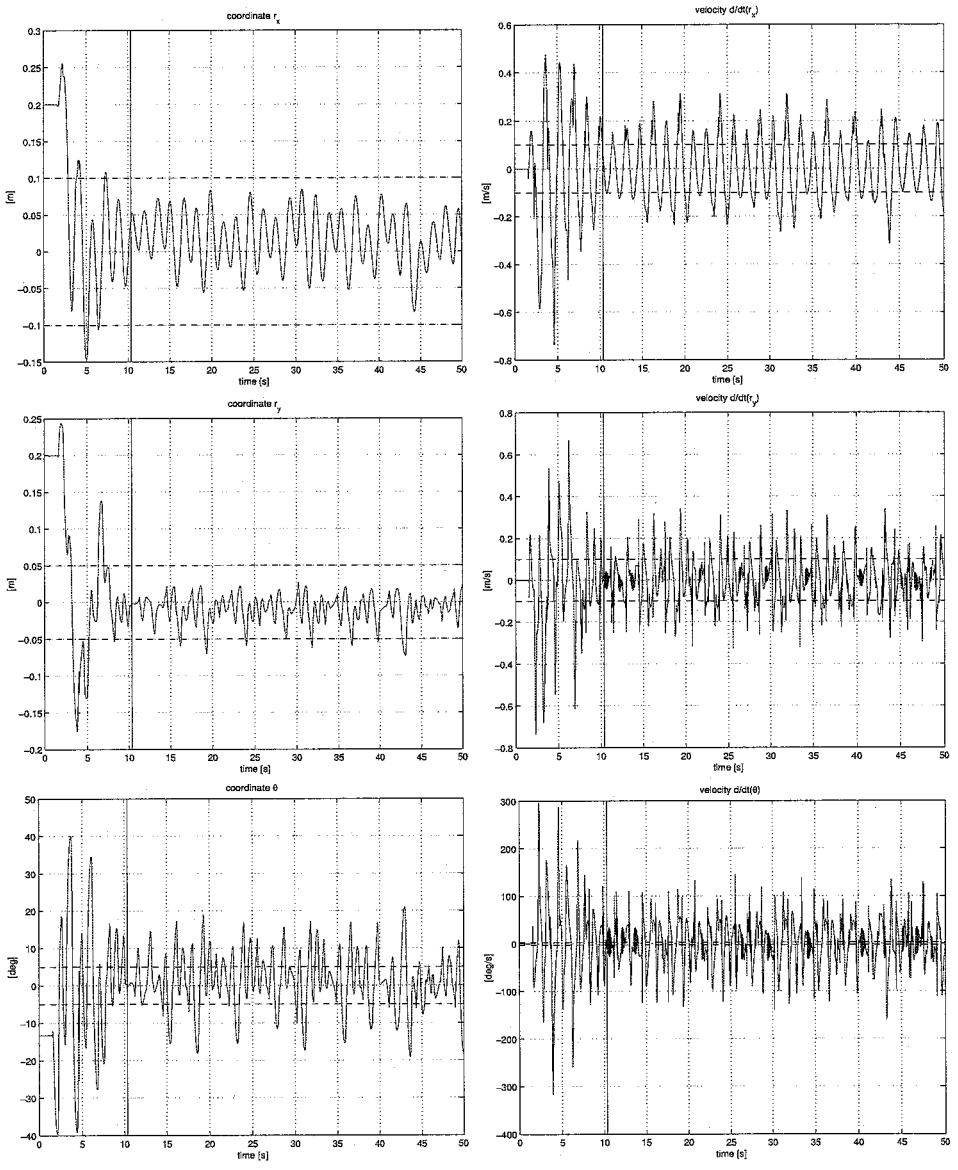

Figure A.7: Continuous measurement with tilted platform, negative initial angle and 0° reference angle.

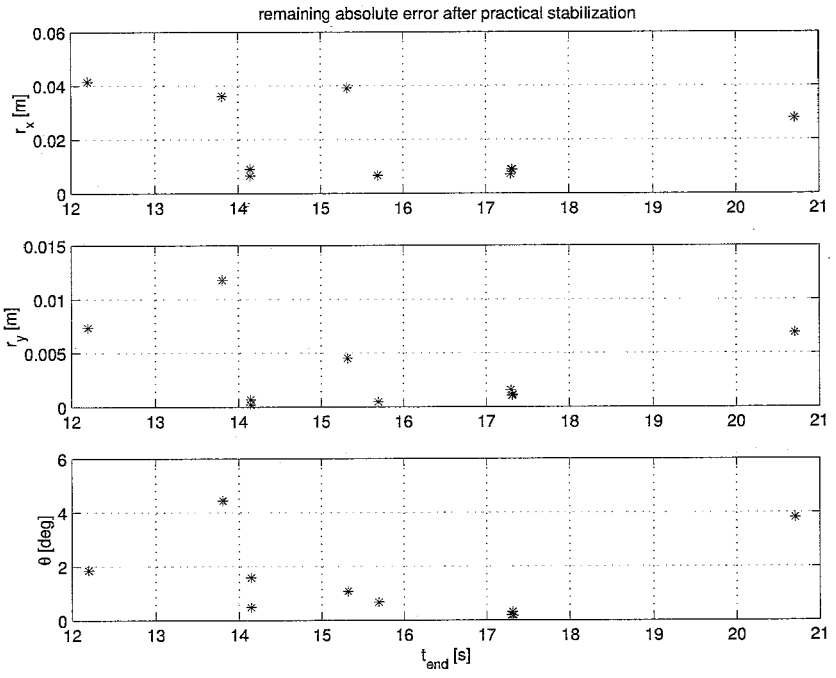

Figure A.8: Relation between the time needed for practical convergence and the absolute remaining error. The measurement is performed with tilted platform, positive initial angle and 0° reference angle.

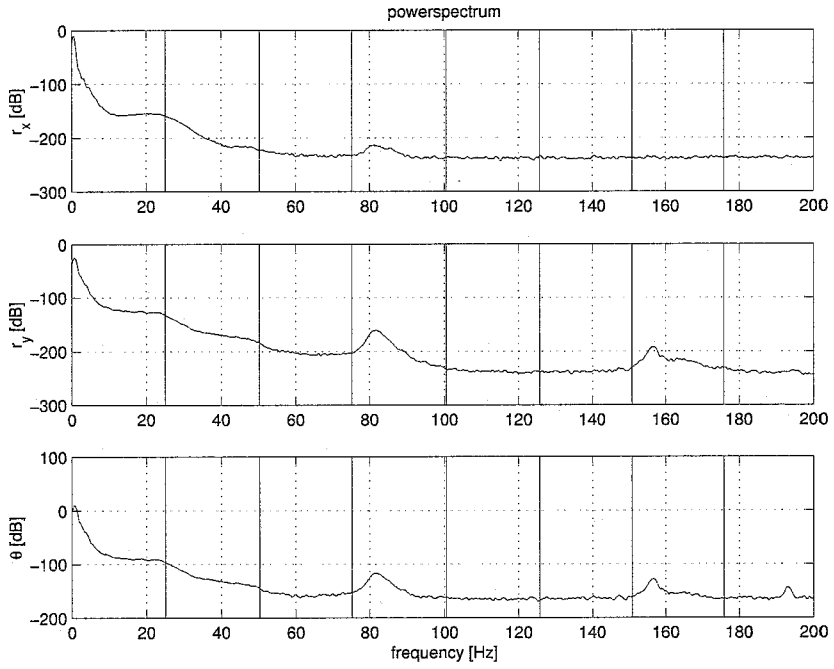

Figure A.9: Powerspectra for r_x, r_y and θ. The harmonics of frequency $\frac{2\pi}{\epsilon}$ Hz are indicated by vertical lines.

A.6 Conclusions

- The levelled platform is influenced by gravitational torque, causing preferential behavior.
- When the platform is slightly tilted the preferential behavior is decreased, but not completely eliminated.
- The effect of an asymmetric friction characteristic is difficult to demonstrate due to the fact that gravitational torque has not been eliminated.
- When practical convergence is not used a sort of periodic motion around the desired state arises. Its amplitude is large compared to the mean remaining errors in similar experiments.

A.7 Recommendations

A possible way to measure the tilt of the axis is to place a small laser-pointer on top of the axis and place a vertical screen around the H-drive. The distance from the laser spot to the ground should be measured at four positions to be able to detect the tilt

around both x and y axis. If the distance from the axis to the screen is known the tilt of the axis can be calculated using standard geometry. The further away the screen can be placed from the axis the more accurate the tilt can be measured.

When it is possible to measure the tilt of the axis new experiments can be conducted with a truly vertical axis. The effects of friction may then be investigated without the trouble of a gravitational torque.

Appendix B

Controllability of the underactuated H-drive including tilt

In [1] the H-drive is modelled as two perpendicular sleds. The X-beam is motorized by two Y-motors that can move independently, but are combined in software to prevent misalignment. The linearization of the dynamics of this system is not fully controllable in any given point in space.

In reality a small misalignment between the Y-motors is possible. The difference in position of the Y-motors introduces a rotational degree of freedom for the X-beam. In figure B.1, this horizontal tilt is indicated by φ. The controllability of the underactuated H-drive might be affected by allowing horizontal tilt of the X-beam. Therefore, the controllability of the linearization of the equations of motion including horizontal tilt will be investigated. Controllability properties will be evaluated by computing the controllability matrix.

B.1 Lagrangian mechanics

The equations of motion will be derived using the Lagrange approach. The Lagrange equation of motion is given by:

$$\frac{d}{dt}\left(T,_{\underline{\dot{q}}}\right) - T,_{\underline{q}} + V,\underline{q} = \left(Q^{nc}\right)^T \tag{B.1}$$

Here, T represents the kinetic energy of the system, V stands for the potential energy and Q represents the generalized forces. The absolute coordinate system $(\vec{\underline{e}})$ is given in figure B.1.

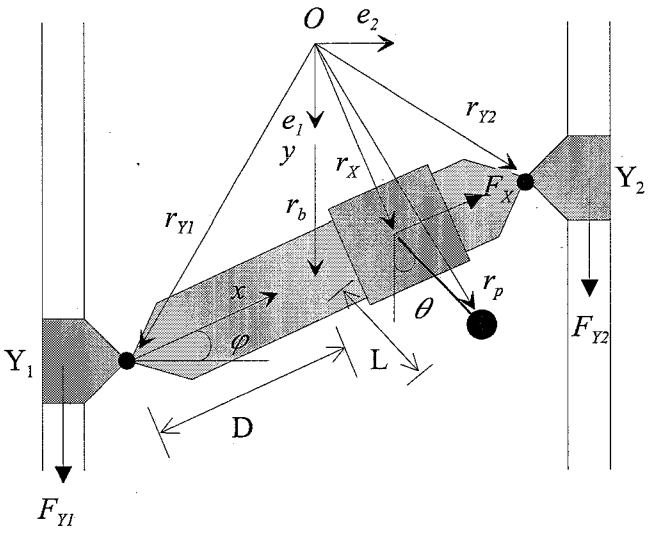

Figure B.1: Top view of the H-drive. The misalignment between the Y-motors has been strongly enlarged for the sake of clearness.

The H-drive is modelled using rigid bodies. The generalized coordinates are chosen as $\underline{q} = [y, \varphi, x, \theta]^T$, the absolute coordinates as $\underline{\vec{e}} = [\vec{e}_1, \vec{e}_2]^T$ and the inputs are given by $\underline{u} = [i_{Y1}, i_{Y2}, i_X]^T$. The position vectors and forces shown in figure B.1 are defined as:

$$\vec{r}_b = \begin{bmatrix} y \\ 0 \end{bmatrix} \underline{\vec{e}}$$

$$\vec{r}_X = \vec{r}_b + (x - D) \begin{bmatrix} -\sin(\varphi) \\ \cos(\varphi) \end{bmatrix} \underline{\vec{e}}$$

$$\vec{r}_{Y1} = \vec{r}_b + D \begin{bmatrix} \sin(\varphi) \\ -\cos(\varphi) \end{bmatrix} \underline{\vec{e}}$$

$$\vec{r}_{Y2} = \vec{r}_b + D \begin{bmatrix} -\sin(\varphi) \\ \cos(\varphi) \end{bmatrix} \underline{\vec{e}}$$

$$\vec{r}_p = \vec{r}_X + L \begin{bmatrix} \cos(\theta) \\ \sin(\theta) \end{bmatrix} \underline{\vec{e}}$$

$$\vec{F}_{Y1} = \begin{bmatrix} 0 \\ k_m i_{Y1} \end{bmatrix} \underline{\vec{e}}$$

$$\vec{F}_{Y2} = \begin{bmatrix} 0 \\ k_m i_{Y2} \end{bmatrix} \underline{\vec{e}}$$

$$\vec{F}_X = \begin{bmatrix} -k_m i_X \\ 0 \end{bmatrix} \underline{\vec{e}}$$

In table B.1 the masses of the various parts of the H-drive are defined. The kinetic

Table B.1: Definition of masses of various parts of the H-drive

mass	description
m_X	X-motor
m_{Y1}, m_{Y2}	Y-motors
m_b	X-beam
m_p	rotating link

energy of the system is given by:

$$\begin{aligned} T &= \frac{1}{2}m_{Y1}\dot{\vec{r}}_{Y1}\cdot\dot{\vec{r}}_{Y1} + \frac{1}{2}m_{Y2}\dot{\vec{r}}_{Y2}\cdot\dot{\vec{r}}_{Y2} + \frac{1}{2}m_X\dot{\vec{r}}_X\cdot\dot{\vec{r}}_X + \\ &\quad \frac{1}{2}m_b\dot{\vec{r}}_b\cdot\dot{\vec{r}}_b + \frac{1}{2}m_p\dot{\vec{r}}_p\cdot\dot{\vec{r}}_p + \\ &\quad \frac{1}{2}I_b\dot{\varphi}^2 + \frac{1}{2}I_p\dot{\theta}^2 \end{aligned} \tag{B.2}$$

The partial derivatives of T w.r.t. $\underline{q}$ and $\dot{\underline{q}}$, as well as the time-derivative $\frac{d}{dt}\left(T_{,\dot{\underline{q}}}\right)$, will be omitted here. The potential energy is zero since no flexibility has been modelled and all degrees of freedom are defined within a plane perpendicular to the plane of gravity. The generalized forces are obtained by:

$$Q^{nc} = \sum_{i=1}^{3}\left(\frac{\partial\vec{r}_i}{\partial\underline{q}}\right)^T\cdot\vec{F}_i \tag{B.3}$$

The Lagrange equations of motion in (B.1) can be rewritten in the following form:

$$\mathbf{M}(\underline{q})\ddot{\underline{q}} + \mathbf{H}(\underline{q},\dot{\underline{q}}) = \underline{Q}^{nc} \tag{B.4}$$

Here, $\mathbf{M}(\underline{q})$ is the mass-matrix, $\mathbf{H}(\underline{q},\dot{\underline{q}})$ contains centripetal and Coriolis terms and $\underline{Q}^{nc}$ represents the applied forces and moments. As a final result of the Lagrange procedure,

the matrix $\mathbf{M}$ and the columns $\mathbf{H}$ and $\underline{Q}^{nc}$ will be given.

$$
\begin{aligned}
\mathbf{M}_{[11]} &= m_{Y1} + m_{Y2} + m_X + m_b + m_p \\
\mathbf{M}_{[12]} &= (m_{Y1} - m_{Y2})D\cos(\varphi) + (m_X + m_p)(D - x)\cos(\varphi) \\
\mathbf{M}_{[13]} &= -(m_X + m_p)\sin(\varphi) \\
\mathbf{M}_{[14]} &= -m_p L \sin(\theta) \\
\mathbf{M}_{[21]} &= (m_{Y1} - m_{Y2})D\cos(\varphi) + (m_X + m_p)(D - x)\cos(\varphi) \\
\mathbf{M}_{[22]} &= (m_p + m_{Y1} + m_{Y2} + m_X + 1/3m_b)D^2 - 2m_p xD + m_x x^2 + m_p x^2 - 2m_x xD \\
\mathbf{M}_{[23]} &= 0 \\
\mathbf{M}_{[24]} &= m_p L \sin(\theta)\cos(\varphi)(x - D) + m_p L \cos(\theta)\sin(\varphi)(D - x) \\
\mathbf{M}_{[31]} &= -(m_X + m_p)\sin(\varphi) \\
\mathbf{M}_{[32]} &= 0 \\
\mathbf{M}_{[33]} &= m_X + m_p \\
\mathbf{M}_{[34]} &= m_p L(\sin(\theta)\sin(\varphi) + \cos(\theta)\cos(\varphi)) \\
\mathbf{M}_{[41]} &= -m_p L \sin(\theta) \\
\mathbf{M}_{[42]} &= m_p L(x - D)\sin(\theta)\cos(\varphi) - m_p L \cos(\theta)\sin(\varphi)(D - x) \\
\mathbf{M}_{[43]} &= m_p L(\sin(\theta)\sin(\varphi) + \cos(\theta)\cos(\varphi)) \\
\mathbf{M}_{[44]} &= m_p L^2 + \frac{1}{1250}
\end{aligned}
\tag{B.5}
$$

$$
\begin{aligned}
\mathbf{H}_{[1]} &= (m_{Y1} - m_{Y2})D\sin(\varphi)\ddot{\varphi}^2 + m_X \sin(\varphi)\ddot{\varphi}^2(D - x) + m_p \sin(\varphi)\ddot{\varphi}^2(D - x) + \\
&\quad + 2(m_X + m_p)\cos(\varphi)\dot{\varphi}\dot{x} + m_p L \cos(\theta)\dot{\theta}^2 \\
\mathbf{H}_{[2]} &= m_p L\dot{\theta}^2 \cos(\varphi)\cos(\theta)(D - x) + m_p L\dot{\theta}^2 \sin(\varphi)\sin(\theta)(D - x) \\
&\quad + 2m_p \dot{x}\dot{\varphi}(D - x) + 2m_X \dot{x}\dot{\varphi}(D - x) \\
\mathbf{H}_{[3]} &= m_p L\dot{\theta}^2(\sin(\theta)\cos(\varphi) - \cos(\theta)\sin(\varphi) + (m_X + m_p)\dot{\varphi}^2(x - D) \\
\mathbf{H}_{[4]} &= m_p L\dot{\varphi}^2(\sin(\theta)\sin(\varphi) + \cos(\theta)\cos(\varphi))(x - D) \\
&\quad + 2m_p L\dot{x}\dot{\varphi}(\cos(\theta)\sin(\varphi) - \sin(\theta)\cos(\varphi))
\end{aligned}
\tag{B.6}
$$

$$
\begin{aligned}
\underline{Q}^{nc} &= \frac{372}{5} k_m \begin{bmatrix} 1 & 1 & -\sin(\varphi) \\ D\cos(\varphi) & -D\cos(\varphi) & 0 \\ 0 & 0 & 1 \\ 0 & 0 & 0 \end{bmatrix} \begin{bmatrix} i_{Y1} \\ i_{Y2} \\ i_X \end{bmatrix} \\
&= \underline{\tau} \cdot \underline{u}
\end{aligned}
\tag{B.7}
$$

B.2 State space representation

The second order differential equations in (B.9) can be written in state space notation using the states $\underline{x}$

$$\underline{x} = \begin{bmatrix} \underline{x}_1 \\ \underline{x}_2 \end{bmatrix} = \begin{bmatrix} \underline{q} \\ \dot{\underline{q}} \end{bmatrix} \tag{B.8}$$

An explicit expression for $\ddot{\underline{q}}$ can be obtained by writing (B.4) in the following form:

$$\ddot{\underline{q}} = -\mathbf{M}^{-1}(\underline{q})\mathbf{H}(\underline{q}, \dot{\underline{q}}) + \mathbf{M}^{-1}(\underline{q})\underline{\tau u} \tag{B.9}$$

The equations of motion then become

$$\dot{\underline{x}} = \underbrace{\begin{bmatrix} x_2 \\ -\mathbf{M}^{-1}(x_1)\mathbf{H}(x_1, x_2) \end{bmatrix}}_{f(x)} + \underbrace{\begin{bmatrix} 0 \\ \mathbf{M}^{-1}(x_1) \end{bmatrix}}_{g(x)} \underline{\tau u} \tag{B.10}$$

The linearization of (B.10) around $\underline{x}_0$ and $\underline{u}_0$ is given by

$$\dot{\tilde{\underline{x}}} = A\tilde{\underline{x}} + B\tilde{\underline{u}} \tag{B.11}$$

where

$$\tilde{\underline{x}} = \underline{x} - \underline{x}_0 \quad , \quad \tilde{\underline{x}} = \underline{x} - \underline{x}_0 \tag{B.12}$$

and

$$A = \frac{\partial f(\underline{x})}{\partial \underline{x}}\Big|_{\underline{x}=\underline{x}_0, \underline{u}=\underline{u}_0} \quad , \quad B = \frac{\partial g(\underline{x})}{\partial \underline{x}}\Big|_{\underline{x}=\underline{x}_0, \underline{u}=\underline{u}_0} \tag{B.13}$$

The linearization will be evaluated around the origin of the absolute coordinate system $\vec{\underline{e}}$. This coincides with the state $\underline{x}_0 = [0, 0, D, 0, \ 0, 0, 0, 0]^T$ and the inputs $\underline{u}_0 = [0, 0, 0]^T$.

B.3 Controllability of the linearized system

The controllability matrix P is defined as

$$P = \begin{bmatrix} B & AB & A^2B & \dots & A^{n-1}B \end{bmatrix} \tag{B.14}$$

The system (B.10) is said to be (locally) controllable when P has full rank. By substituting the numerical values given in table (B.2), the computation of P is considerably facilitated. Finally, P is given by:

$$P = \begin{bmatrix} 0 & 0 & 0 & 1.25 & 1.25 & 0 & 0 & \dots & 0 \\ 0 & 0 & 0 & 8.57 & -8.57 & 0 & 0 & \dots & 0 \\ 0 & 0 & 0 & 0 & 0 & 8.14 & 0 & \dots & 0 \\ 0 & 0 & 0 & 0 & 0 & -28.73 & 0 & \dots & 0 \\ 1.25 & 1.25 & 0 & 0 & 0 & 0 & 0 & \dots & 0 \\ 8.57 & -8.57 & 0 & 0 & 0 & 0 & 0 & \dots & 0 \\ 0 & 0 & 8.14 & 0 & 0 & 0 & 0 & \dots & 0 \\ 0 & 0 & -28.73 & 0 & 0 & 0 & 0 & \dots & 0 \end{bmatrix} \tag{B.15}$$

Table B.2: Numerical values

parameter	value
D	0.3 [m]
L	0.15 [m]
m_{Y1}	9.12 [kg]
m_{Y2}	9.12 [kg]
m_X	9.12 [kg]
m_p	0.04 [kg]
m_b	32.08 [kg]

P does not have full rank; its rank equals 6. Since rank(P) is not equal to $n = 8$, the linearization of the system given by (B.10) is not controllable. Concluding, the introduction of tilt of the X-beam in the equations of motion does not make the origin of the linearized system fully controllable. A physical explanation for this is given by the fact that the H-drive moves in a plane which is perpendicular to the gravity vector. As a consequence, the origin is no asymptotically stable equilibrium point. If the H-drive would move in a plane parallel to the gravity vector, gravity would contribute to move the link towards the origin; the origin would be an asymptotically stable equilibrium point. Then, the system would be fully controllable. Note that in case of the vertical configuration only the origin is controllable.